



National Library
of Canada

Bibliothèque nationale
du Canada

Canadian Theses Service

Services des thèses canadiennes

Ottawa, Canada
K1A 0N4

CANADIAN THESES

THÈSES CANADIENNES

NOTICE

The quality of this microfiche is heavily dependent upon the quality of the original thesis submitted for microfilming. Every effort has been made to ensure the highest quality of reproduction possible.

If pages are missing, contact the university which granted the degree.

Some pages may have indistinct print especially if the original pages were typed with a poor typewriter ribbon or if the university sent us an inferior photocopy.

Previously copyrighted materials (journal articles, published tests, etc.) are not filmed.

Reproduction in full or in part of this film is governed by the Canadian Copyright Act, R.S.C. 1970, c. C-30.

**THIS DISSERTATION
HAS BEEN MICROFILMED
EXACTLY AS RECEIVED**

AVIS

La qualité de cette microfiche dépend grandement de la qualité de la thèse soumise au microfilmage. Nous avons tout fait pour assurer une qualité supérieure de reproduction.

S'il manque des pages, veuillez communiquer avec l'université qui a conféré le grade.

La qualité d'impression de certaines pages peut laisser à désirer, surtout si les pages originales ont été dactylographiées à l'aide d'un ruban usé ou si l'université nous a fait parvenir une photocopie de qualité inférieure.

Les documents qui font déjà l'objet d'un droit d'auteur (articles de revue, examens publiés, etc.) ne sont pas microfilmés.

La reproduction, même partielle, de ce microfilm est soumise à la Loi canadienne sur le droit d'auteur, SRC 1970, c. C-30.

**LA THÈSE A ÉTÉ
MICROFILMÉE TELLE QUE
NOUS L'AVONS REÇUE**

THE UNIVERSITY OF ALBERTA

AN EXPERIMENTAL AND NUMERICAL ANALYSIS
OF ORTHODONTIC T SPRINGS

by

PETER FUCHSHUBER

(C)

A THESIS

SUBMITTED TO THE FACULTY OF GRADUATE STUDIES AND RESEARCH
IN PARTIAL FULFILMENT OF THE REQUIREMENTS FOR THE DEGREE
OF MASTER OF SCIENCE

DEPARTMENT OF MECHANICAL ENGINEERING

EDMONTON, ALBERTA

SPRING 1987

Permission has been granted to the National Library of Canada to microfilm this thesis and to lend or sell copies of the film.

The author (copyright owner) has reserved other publication rights, and neither the thesis nor extensive extracts from it may be printed or otherwise reproduced without his/her written permission.

L'autorisation a été accordée à la Bibliothèque nationale du Canada de microfilmer cette thèse et de prêter ou de vendre des exemplaires du film.

L'auteur (titulaire du droit d'auteur) se réserve les autres droits de publication; ni la thèse ni de longs extraits de celle-ci ne doivent être imprimés ou autrement reproduits sans son autorisation écrite.

ISBN 0-315-37746-1

THE UNIVERSITY OF ALBERTA

RELEASE FORM

NAME OF AUTHOR PETER FUCHSHUBER
TITLE OF THESIS AN EXPERIMENTAL AND NUMERICAL ANALYSIS
 OF ORTHODONTIC T SPRINGS
DEGREE FOR WHICH THESIS WAS PRESENTED MASTER OF SCIENCE
YEAR THIS DEGREE GRANTED SPRING 1987

Permission is hereby granted to THE UNIVERSITY OF ALBERTA LIBRARY to reproduce single copies of this thesis and to lend or sell such copies for private, scholarly or scientific research purposes only.

The author reserves other publication rights, and neither the thesis nor extensive extracts from it may be printed or otherwise reproduced without the author's written permission.

(SIGNED)

Peter Fuchshuber

PERMANENT ADDRESS:

9820 169 Street

Edmonton, Alberta

T5P 3X4

DATED April 3 1987

THE UNIVERSITY OF ALBERTA

FACULTY OF GRADUATE STUDIES AND RESEARCH

The undersigned certify that they have read, and recommend to the Faculty of Graduate Studies and Research, for acceptance, a thesis entitled AN EXPERIMENTAL AND NUMERICAL ANALYSIS OF ORTHODONTIC T SPRINGS submitted by PETER FUCHSHUBER in partial fulfilment of the requirements for the degree of MASTER OF SCIENCE.

Gary Faulkner

Supervisor

Don Habert

William

Kenneth E. Sker

Date April 3, 1987

Dedicated to my parents

ABSTRACT

Orthodontic springs are used to deliver forces and moments to teeth to achieve tooth movement. The desired movement will only occur provided that the proper force systems, which fall into a narrow, physiologically acceptable range, are generated by the appliance. The determination of the force-deflection behaviour of a particular spring design is therefore essential to the development of an appliance. This work attempts to determine this behaviour from both experimental and numerical approaches.

An instrument capable of measuring the force systems produced by orthodontic springs was developed using strain gauge based transducers to sense the three-dimensional forces and moments. A large displacement finite element analysis of the deformation of the springs was conducted. Experimental and numerical results for the activation of two appliances were compared. The instrument was also applied in further studies to determine the effects of varying several geometric parameters in a T loop design.

Acknowledgements

I wish to thank Dr. M.G. Faulkner for his guidance and invaluable advice in seeing this thesis to its completion. I would also like to thank Dr. D.L. Haberstock for his interest and involvement throughout this project. Mr. A. Hay and Mr. T. Kaiser are also thanked for their assistance.

Thanks are also extended to Mr. T. Vanstraten, Mr. A. Yuen, and Mr. B. Cielin of the machine shop at the Department of Mechanical Engineering. Funding for the project was provided by the Natural Sciences and Engineering Research Council of Canada (NSERC grant A7514).

Table of Contents

Chapter	Page
1. INTRODUCTION	1
1.1 Orthodontic Background	1
1.2 Thesis Outline	3
1.3 Experimental Studies	5
1.4 Numerical Studies	7
2. EXPERIMENTAL EQUIPMENT	15
2.1 Design Concepts and Details	15
2.2 System Test Results	24
3. FINITE ELEMENT THEORY	29
3.1 Formulation of Equilibrium Equations	29
3.2 Solution Strategy	33
3.3 Convergence Criteria	36
3.4 Isoparametric Beam Element	36 ^e
4. TEST RESULTS	42
4.1 Comparative Studies	42
4.2 Parametric Studies	54
5. CONCLUSIONS	73
REFERENCES	76
APPENDIX	79

List of Figures

Figure	Page
1.1 Segmented arch approach to space closure	2
1.2 Free-body diagram of separated archwire	8
1.3 Illustration of midpoint tangent incremental (MTI) solution	8
2.1 Schematic and free-body diagram of system	20
2.2 Strain distribution on upper surface of 'binocular' cantilever	22
2.3 Cantilever dimensions	22
2.4 Variation of sensitivity with cutout diameter	23
2.5 Force test results	25
2.6 Moment test results	25
2.7 Force cross-talk resulting from applied force	26
2.8 Moment cross-talk resulting from applied force	26
2.9 Deflection of sensing mount with load	28
3.1 Modified Newton-Raphson iterative solution for increment in displacements	35
3.2 BFGS solution	35
3.3 Coordinate systems and position vectors for isoparametric beam element	39
3.4 Two-dimensional, two-node illustration of coordinate interpolations	39
4.1 T spring with no pre-activation	43

4.2	Original and deformed finite element mesh	43
4.3	Force-deflection relationships	45
4.4	Moment-deflection relationships	46
4.5	Pre-activated T spring	48
4.6	Prescribed rotation and displacement of spring end	48
4.7	Finite element mesh	49
4.8	Force vs. deflection from neutral position	51
4.9	Moment vs. deflection from neutral position	52
4.10	Calculated force-deflection relationships	53
4.11	Calculated moment-deflection relationships	53
4.12	Spring height variation	55
4.13	Force-deflection relationship	55
4.14	Moment-deflection relationship	57
4.15	Moment to force ratio vs. deflection from neutral position	57
4.16	Changes in activation angle	58
4.17	Horizontal force	58
4.18	Vertical force at α end	60
4.19	Moment at α end	60
4.20	Moment at β end	61
4.21	Moment to force ratio at α end	61
4.22	Moment to force ratio at β end	62
4.23	Variation in clamping points	65
4.24	Horizontal force	65
4.25	Vertical force at α end	66
4.26	Moment at α end	66

4.27 Moment at β end67
4.28 Moment to force ratio at β end67
4.29 Moment to force ratio at β end68
4.30 Addition of helices70
4.31 Horizontal force-deflection relationship70
4.32 Moment-deflection relationship.....72
4.33 Moment to force ratio72

List of Plates

Plate	Page
2.1 Load cell for determining three-dimensional force systems	17
2.2 Close-up showing displacement mount and cross resolver	19

Nomenclature

u	nodal displacement vector
R	nodal load vector
K	stiffness matrix
Σ_0	initial stress matrix
b	nodal force and displacement vector
p	external load vector
u	displacement of a particle in a body
H	displacement <u>interpolation</u> matrix
B	strain-displacement interpolation matrix
t_K^l, t_K^{nl}	linear and initial stress incremental stiffness matrices at time t
Δu	vector of increments in nodal displacements
$t+\Delta t_R$	vector of externally applied loads at $t+\Delta t$
$t+\Delta t_F$	vector of nodal point forces determined from integration of internal stresses

1. INTRODUCTION

1.1 Orthodontic Background

Orthodontic springs are used to move teeth in order to improve occlusion and esthetics. This is achieved through the delivery of forces and moments to the teeth. The movement of a tooth may involve three-dimensional displacements and rotations and the required force and moment system is usually complex. A moment is usually required even for a pure translation of the tooth as the point of force application seldom coincides with the tooth's center of resistance. In addition, the movement of teeth is due to the resorption and apposition of bone tissue in response to pressure and tension applied within a physiologically acceptable range. Thus the requirements on the force-deflection behaviour of orthodontic springs are many and the prediction of the characteristics of these appliances is important.

The primary function performed by orthodontic springs is the closure of space in the dental arch. One of the more recent ways this has been achieved is through the use of the segmented arch technique. In this approach groups of teeth are banded together to create anterior and posterior segments and a spring is attached and activated between these segments. This technique is illustrated schematically in Figure 1.1. The springs are typically

Figure 1.1 Segmented arch approach to space closure

made from stainless steel or from TMA (titanium molybdenum alloy). Characteristic of TMA is its low modulus of elasticity, broad elastic range and high ultimate strength. Tooth displacements range from 0.5 mm to 7 mm and the maximum forces and moments delivered to the tooth are typically 2-2.5 N and 25-30 N-mm (1 N = 102 gf). The T loop spring shown in Figure 1.1 is a frequently used design for retracting teeth towards the back of the mouth. This is because it provides a suitable ratio of moment to force delivery to achieve tooth translation without causing excessive rotation. This spring design was the focus of this study.

1.2 Thesis Outline

The intent of this study was to develop and apply an instrument capable of measuring the force systems produced by orthodontic springs, to conduct a numerical analysis of the deformation of the springs and to compare the results from these techniques. In addition, an experimental study to determine the effects of varying certain geometric parameters in a T loop design was done.

The remainder of chapter one reviews recent experimental and numerical analyses that have been performed on orthodontic appliances. Chapter two describes the instrument design, its calibration and capabilities. It concludes with suggestions on possible additions to the

system in order to improve the measurement process.

Chapter three contains theoretical considerations for the finite element study. The program ADINA was used to model the springs. The formulation of the equations of equilibrium is discussed followed by an outline of the solution strategy. The beam element formulation is also described.

The numerical and experimental studies that were conducted are described in chapter four. Two comparative studies were carried out. The first involved the testing and simulation of a non-preactivated T spring. The results were compared to experimental and numerical results obtained using the experimental apparatus reported by Solonche [1] and the program described by Koenig [2]. In clinical applications however, these springs are given preactivation bends and the resulting shape is capable of undergoing far larger displacements and rotations before yielding occurs. The second study then, was an experimental and theoretical analysis of a preactivated spring and allowed a comparison of these two approaches when large displacements were present. The remaining studies were experimental investigations to determine the effect of varying spring height, activation angle, offset mounting and the use of helices in the design.

The final chapter lists the conclusions of the study and suggests possible areas of future research.

1.3 Experimental Studies

Numerous instruments have been designed since 1920 for the purpose of determining the force-deflection relationships of orthodontic appliances. Most early force transducers were balances in which one end of the appliance deflected a calibrated spring element over a sufficiently large displacement or rotation to allow for direct observation. Depending upon the magnitude of the spring element deflection, an error was introduced by not considering the relative displacement between the ends of the appliance. In 1933 a cathetometer was used by Peyton [3] as a means to observe the actual appliance deflection under the application of a known weight. A summary of many early instruments may be found in a paper by Paulich published in 1939 [4].

More recently, strain gauges and electrical displacement transducers have been utilized. In 1953 Johns [5] designed an instrument with a strain gauge which was capable of measuring uniplanar forces and moments. In 1963 Teasly [6] designed an instrument capable of measuring three-dimensional force systems. It utilized six strain gauges and had a measurement accuracy of better than 2 percent. Two more recent devices were reported by Solonche in 1977 [1] and Paquien in 1978 [7].

The instrument discussed by Solonche senses forces through the displacement of a cantilever beam and moments

through the rotation of a torsion bar. The appliance is mounted in two chucks. Each chuck is attached to an angular displacement transducer and a torsion rod. Each transducer is mounted on a cantilever beam whose vertical deflections are monitored with an LVDT. One of the beams is mounted on a moveable carriage which activates the appliance. The linear transducer was calibrated against a gauge block. The remainder of the system was calibrated with deadweights. The individual transducers had repeatability and linearity of less than 1 percent. The instrument has been utilized in several studies [8,9,10].

The second instrument [7] employs strain elements to sense the forces exerted on a triangular base plate onto which one end of the appliance is mounted. The beams are oriented and attached to the plate in such a way as to resolve the force system delivered to the plate into three vertical forces and three horizontal forces parallel to the sides of the equilateral triangle. The six forces are combined to give the three orthogonal forces and moments. Tests indicated that the system measured forces and moments with an accuracy of better than 3 percent full scale.

Three of the beams are positioned with narrow edges as the upper and lower surfaces and are clamped at both ends. The other three are positioned with broad edges to the top and bottom and are inserted into horizontal slots so as to provide purely vertical reactions to the triangular plate. However it is reported that some friction is present at the

slots. This is overcome by attaching the base plate to a vibration source before readings are taken. The device has been used in a comparison study of several archwires [11] and in a study of retraction springs [12].

1.4 Numerical Studies

Prior to 1970 analytical studies of orthodontic appliances had been limited to idealized geometries for which closed form solutions exist. Since then several approaches have been taken to analyze complex springs. Four prominent studies were conducted by Waters in 1970 [13], Yang and Baldwin in 1974 [15], Koenig and Burstone in 1974 [2], and Greif et al. in 1982 [19].

The approach taken by Waters [13] was to idealize the appliance as an assembly of straight beams and then separate them and analyze each with simple beam theory. The procedure is seen in the treatment of a looped span subjected to a central load [13]. The free-body diagram of each component in half of the symmetric spring is shown in Figure 1.2. The moment M was solved for by proceeding along the structure and summing the individual contributions to the rotation and noting that $\theta_{AE} = \theta_{EF}$ (alternatively Castigliano's theorem could have been directly applied). The deflection at F is found in a similar manner. The approach is, of course, limited to those appliances that may be idealized as consisting of

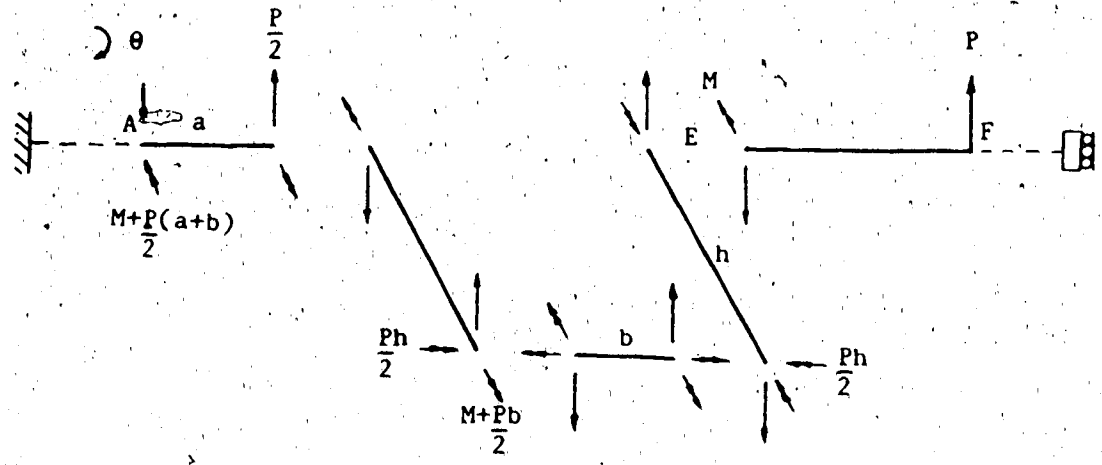


Figure 1.2 Free-body diagram of separated archwire

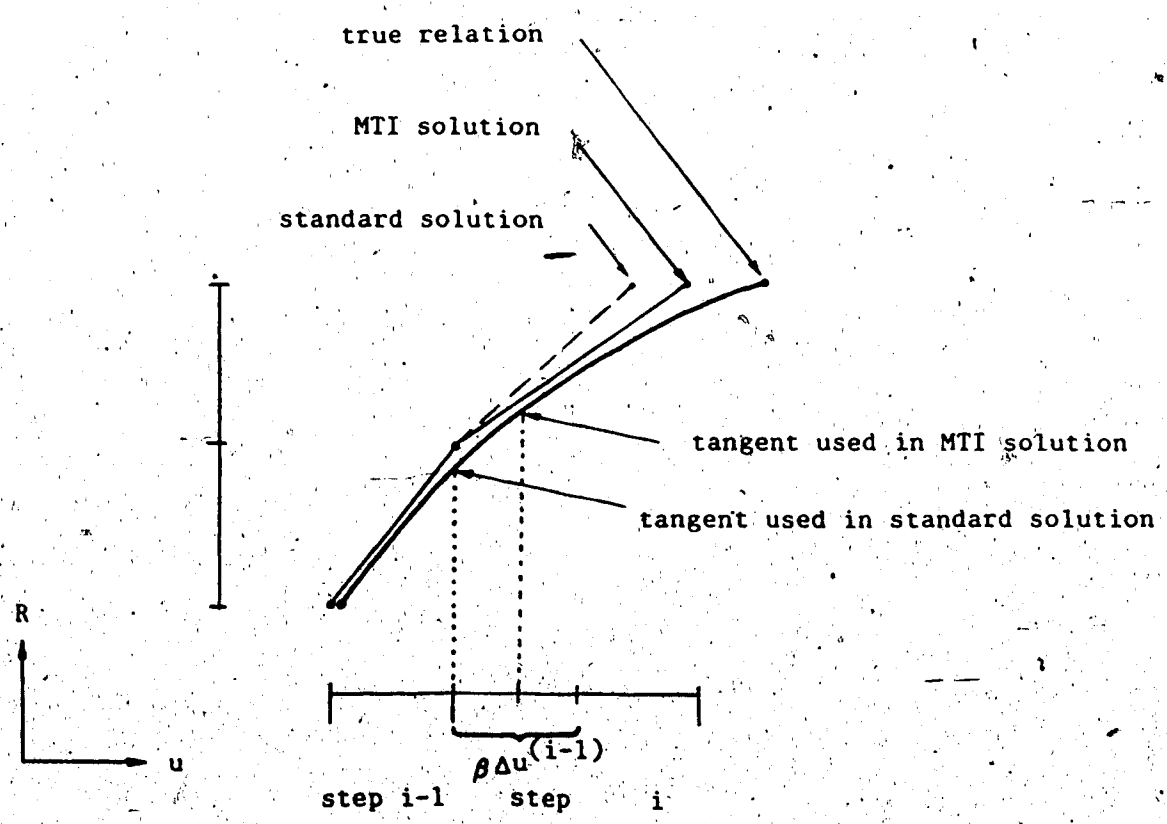


Figure 1.3 Illustration of midpoint tangent incremental (MTI) solution

straight beam elements and that undergo sufficiently small rotations for simple beam theory to apply.

In a paper published in 1973 [14] Yang gave a finite element procedure for solving the large displacement problems of beams and frames. It was later applied to orthodontic appliances. The stiffness formulation was based on small deflections. Geometric nonlinearity was handled with a midpoint tangent incremental solution procedure.

The beam elements formulated were straight two-node elements. The stiffness formulation was carried out with respect to a local coordinate system obtained by rotating the reference axes to coincide with the tangent and normal directions to the beam axis. The nodal force-displacement relationship obtained is

$$[K_1 + \sigma_{01}] u_1 = R_1 \quad (1.1)$$

where u_1 and R_1 are the force and displacement vectors at the nodes with respect to the local coordinate system, K_1 is the stiffness matrix and σ_{01} is the initial stress matrix. This corresponds to a total formulation. At each load step the rotation of the local coordinate system changes, so each element formulation is transformed to a set of reference axes at each step using a transformation matrix. The transformed force-displacement relationships are then assembled into the overall stiffness

equation

$$[K + \Sigma_0] u = R \quad (1.2)$$

An incremental solution procedure was used to solve (1.2). The linearized incremental formulation was obtained by replacing u and R with incremental vectors. The equation obtained is

$$[K^{(i-1)} + \Sigma_0^{(i-1)}] \Delta u^{(i)} = \Delta R^{(i)} \quad (1.3)$$

where i denotes the particular load step. The stiffness matrix and initial stress matrix are both dependent on the rotation of the local coordinate system (ie. the displaced configuration). In addition, the initial stress matrix is dependent on the element axial forces which are also dependent on the displaced configuration. If the load increments are prescribed, the displacements may be solved for using

$$\Delta u^{(i)} = [K^{(i-1)} + \Sigma_0^{(i-1)}]^{-1} \Delta R^{(i)}$$

or conversely if some displacements are prescribed the matrices can be rearranged and partitioned to apply these conditions. Finally, Yang noted that the solution could be improved if the matrices are not based entirely on the displacements at step $i-1$ but rather are based on the

average of the displacements at $i-1$ and the displacements obtained by adding $\beta \Delta u^{(i-1)}$ to these displacements where β is the ratio between the load increments at step i and $i-1$. He called this solution technique the midpoint tangent incremental approach. It is illustrated in Figure 1.3 for the case $\beta=1$.

In a subsequent paper [15] Yang and Baldwin applied this procedure to a vertical loop spring and a more complex design with multiple helices. The vertical loop was subjected to a prescribed end displacement. Good agreement was seen between the nonlinear calculation and experimental results. The complex spring was subjected to a prescribed load. The nonlinear analysis overestimated the resulting displacement by about 8 percent.

In a paper published in 1974 [2] Koenig and Burstone gave a finite difference technique for predicting the load-displacement characteristics of arbitrarily curved and twisted beams. The analysis was initially used in a study of turbine blades in aircraft and was later developed into an incremental nonlinear analysis for predicting the large displacement response of orthodontic appliances.

The appliance is discretized into two-node elements. The equations of motion are based on work on generalized beam theory by von Trostel [16], Suhubi [17] and Massoud [18]. The equations are written in a local coordinate system consisting of the tangent, normal and binormal directions. The discretized equilibrium equations for an

element and the load-deformation equations are written as the matrix equation

$$\alpha_{m-1} b_{m-1,R} = \alpha_m b_{m,L} \quad (1.4)$$

where

$$b^T = [M_t \ M_b \ M_n \ Q_t \ Q_b \ Q_n \ \phi_t \ \phi_b \ \phi_n \ w_t \ w_b \ w_n]$$

M , Q , ϕ and w denote moment, shear force, rotation and displacement and t, b, n denote components in the tangent, binormal and normal local coordinate system (m denotes node number and R and L the left or right surface vector for the cross-section at a node). The conditions of equilibrium and displacement continuity at a node are expressed in matrix form as

$$\alpha_m b_{m,L} = b_{m,R} + P_m \quad (1.5)$$

where P_m is a vector containing the external loads. Substituting $b_{m,L}$ from equation (1.5) into (1.4) yields

$$b_{m-1,R} = \alpha_{m-1}^{-1} \alpha_m \gamma_{m-1} [b_{m,R} + P_m] \quad (1.6)$$

which relates the loads and displacements at a node to

those at the preceding node. By applying equation (1.5) to the first node and equation (1.6) to the remaining nodes and progressively substituting into equation (1.5) the following matrix equation results

$$\underline{Q} b_{N,R} = \gamma_0 b_{0,L} + \lambda \quad (1.7)$$

where 0 denotes the first node and N the last node. The system matrix equation then, contains only the forces and displacements at the first and last nodes.

The boundary conditions of the problem are then expressed in the local coordinate systems at the end points of the appliance and divided into equal increments. The geometric parameters are then computed for the configuration. The incremental boundary conditions are then applied and the system matrix equation is solved. The nodal loads and displacements at the other nodes are then computed and transformed into the global coordinate system. The new geometry and nodal loads serve as the initial conditions for the next step. The procedure is repeated until the boundary conditions have been fully applied. The nodal forces from each step are added to determine the final values.

The nonlinear analysis has been carried out on several appliances and compared to the linear analysis (the linear results were obtained by performing an analysis in a single step). For a vertical loop spring subjected to horizontal

and displacements the nonlinear results predicted a force 4 percent higher and a moment 10 percent lower than the linear results.

In a paper published in 1982 [19] Greif et al. described a three-dimensional finite element approach in which orthodontic springs were modelled with straight beam elements. To analyze geometrically nonlinear problems, an updated Lagrangian incremental formulation (ULF) was used with an iterative (Newton-Raphson) procedure. The technique was applied in the analysis of a uniform archwire. Good agreement was seen between the solution and experimental results. This approach is in parallel with the present numerical study. In the present study a total Lagrangian incremental formulation (TLF) is used with a quasi-Newton iterative procedure. The method is described in chapter three.

2. EXPERIMENTAL EQUIPMENT

The system was designed to measure the forces and moments at one end of an appliance with minimal deflection in comparison to the displacements at the other end so that only those displacements need be measured. Non-symmetric springs can be evaluated by reversing them to measure the forces and moments at both ends. The initial design specifications were that triaxial forces of up to 10 N could be measured with a resolution of 0.05 N, and moments of up to 50 N-mm be measured with a resolution of 0.25 N-mm. The displacements were to be measured with a resolution of 0.1 mm as spring positioning could only be achieved to an accuracy of 0.5 mm at best.

2.1 Design Concepts and Details

The system consists of a load cell attached to a Vishay Ellis 20 scanner/bridge. The strain gauge data is reduced using an IBM PC producing the actual forces and moments. The cell is shown in Plates 2.1 and 2.2. A schematic is also shown in Figure 2.1. A crosspiece is used to resolve the forces and moments at the clamping point into six reaction forces. The dimensions of the resolver were determined by the required resolutions and force transducer capabilities. The resolver is suspended by fine braided wire from six pairs of 'binocular' strain

Plate 2.1 Load cell for determining three-dimensional force systems

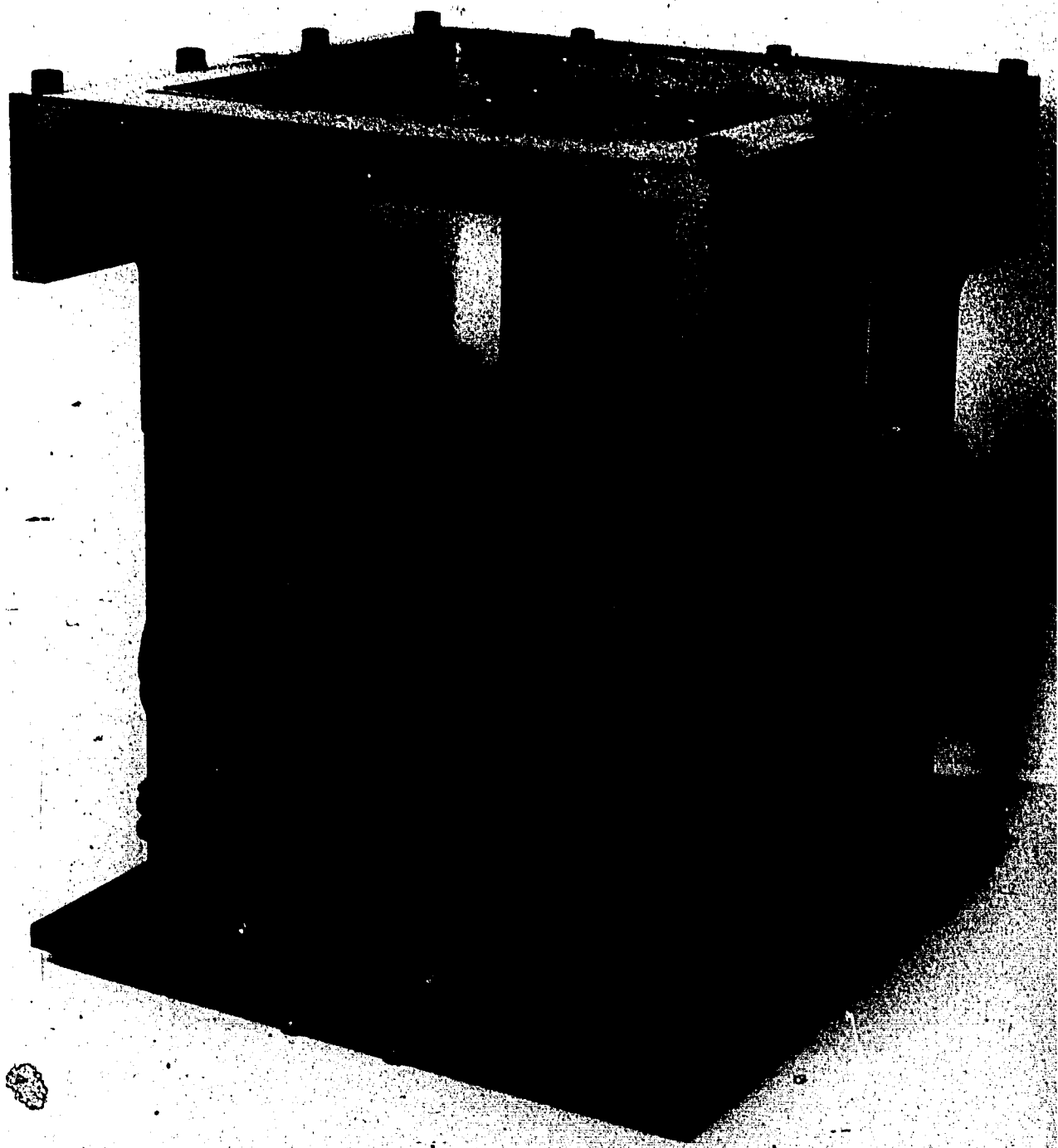


Plate 2.2 Close-up showing displacement mount and cross resolver



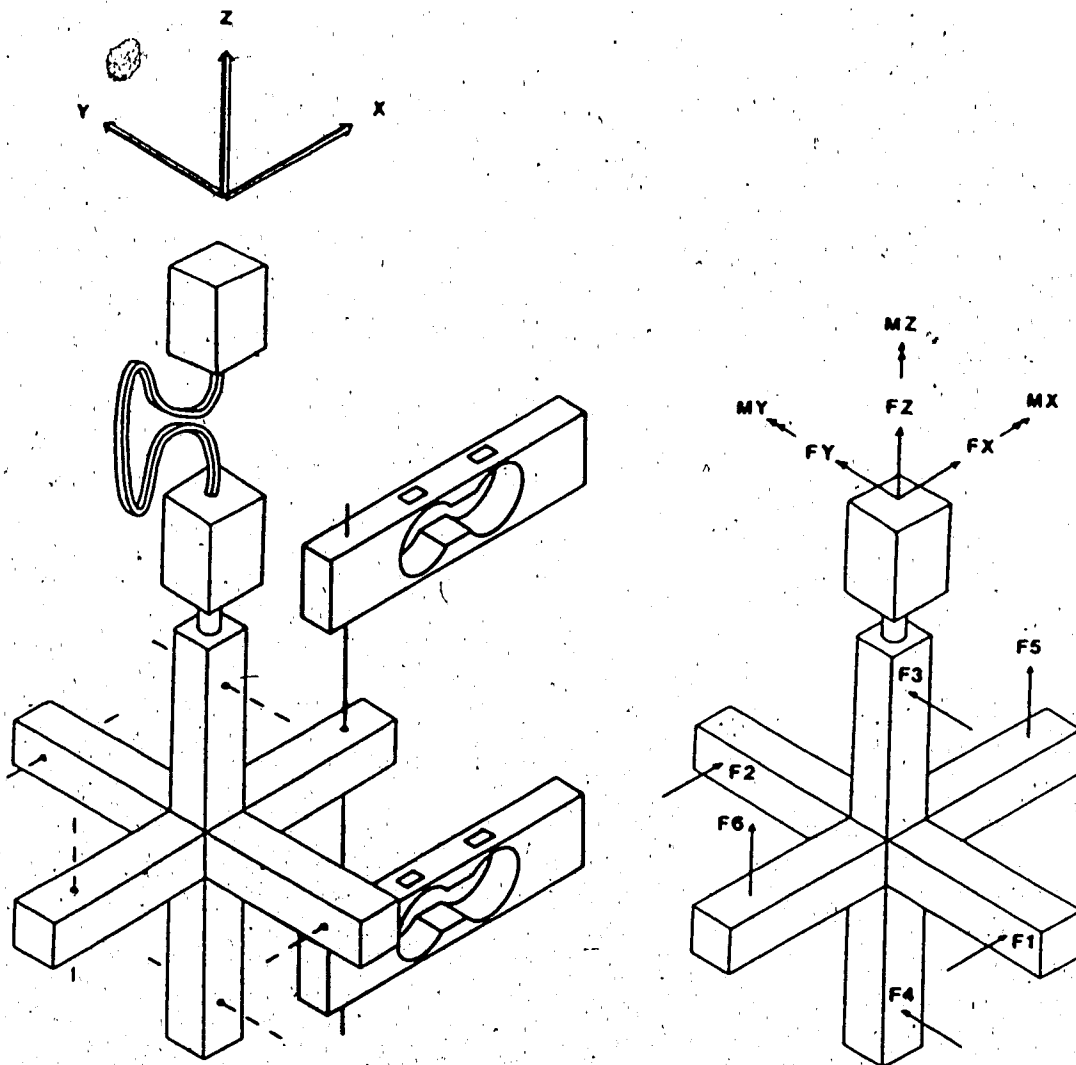


Figure 2.1 Schematic and free-body diagram of system

cantilevers (one pair is shown). These transducers utilize a binocular shaped cutout which creates high strain in the thin sections while maintaining a relatively low deflection. The strain distribution is shown in Figure 2.2.

The transducer dimensions are shown in Figure 2.3. The diameter of the cutout was chosen to give the desired sensitivity and force accommodation. Four transducers of various hole diameters (10.3, 11.1, 11.5 and 11.9 mm) were constructed from 6061 aluminum and tested by applying dead weights. The variation of sensitivity with diametral change is shown in Figure 2.4, indicating the large variations in sensitivity possible with a small change in diameter. For measurement of the F3 force (Figure 2.1), a diameter of 11.1 mm was chosen to accommodate the larger forces expected at this location on the cross resolver; all other forces were measured with transducers using an 11.5 mm diameter. At an applied force of 5 N the maximum departure from linearity for the 11.1 mm transducer was 1.1 percent and for the 11.5 mm transducer 1.8 percent.

The ten 11.5 mm diameter transducers were tested individually and matched into pairs. All six pairs were then mounted individually and calibrated in the 'positive' and 'negative' direction. The wire was pre-tensioned to approximately one half the transducer's linear range. A block was clamped to the wire. Further weight was added to the block. The tests revealed that the transducer pairs did not behave as simple parallel spring systems

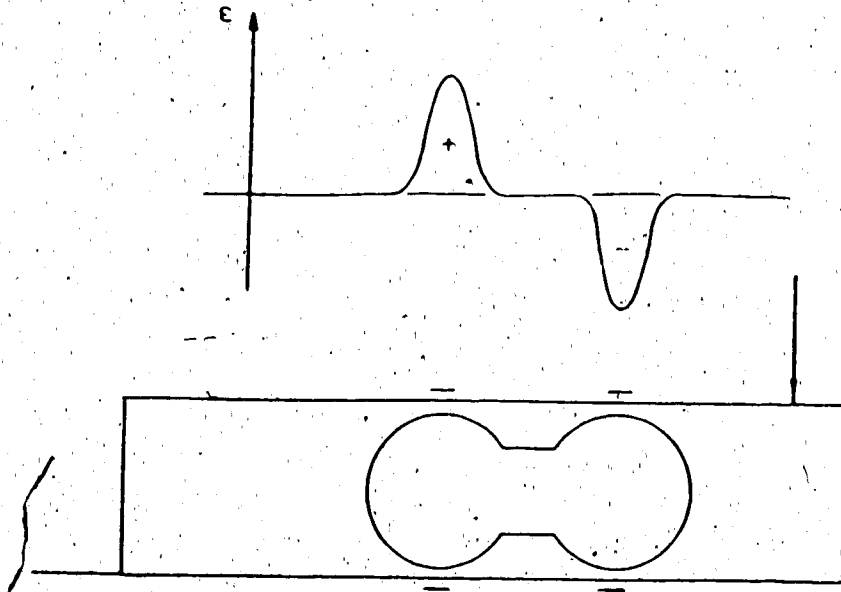


Figure 2.2 Strain distribution on upper surface of 'binocular' cantilever

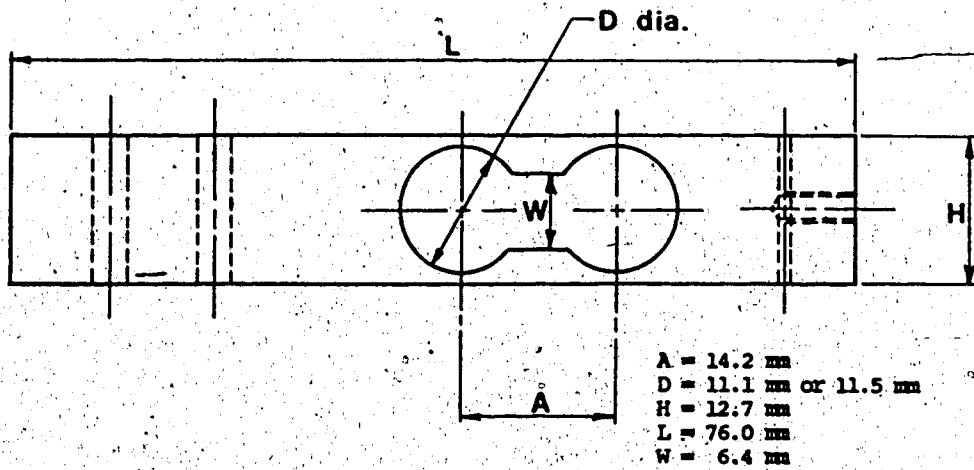


Figure 2.3 Cantilever dimensions

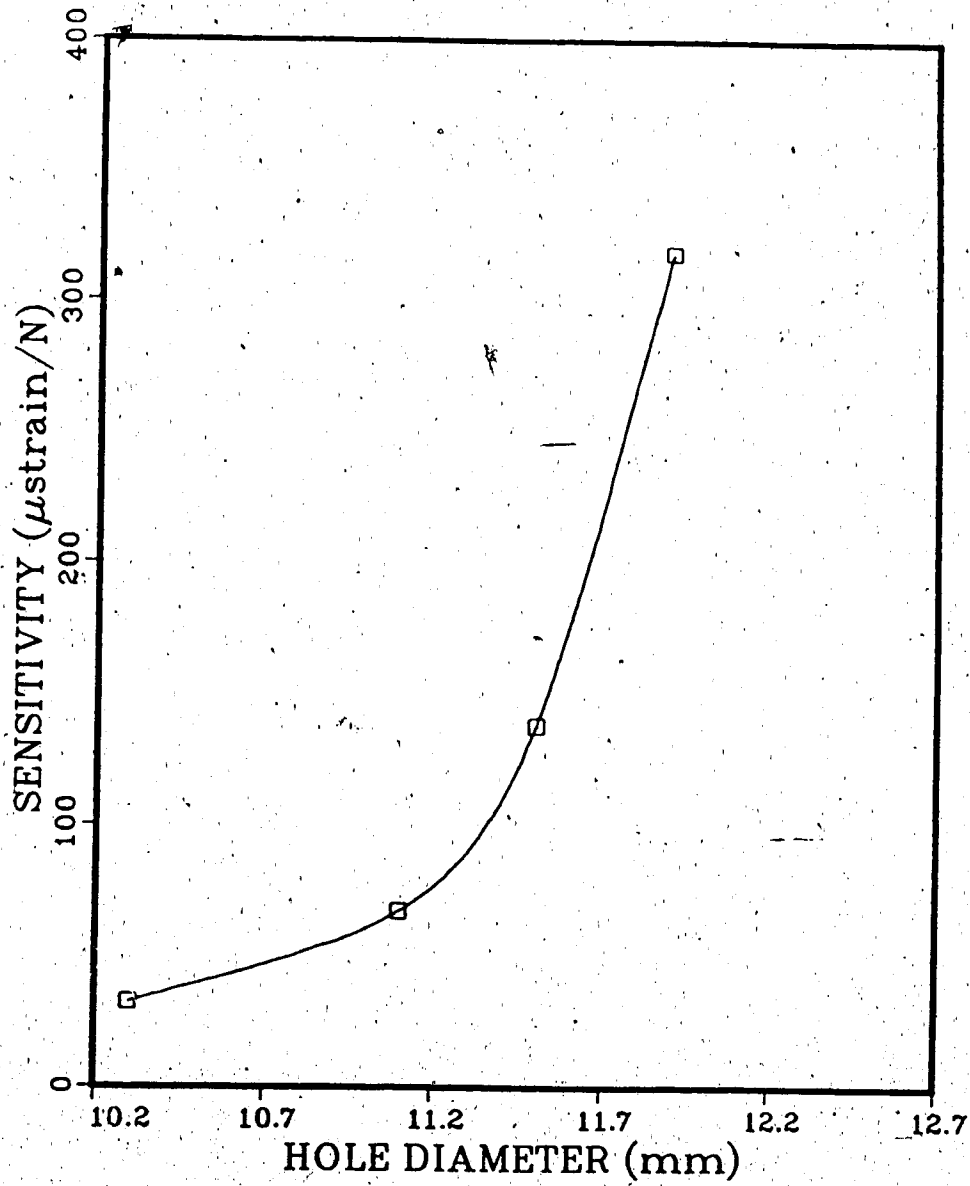


Figure 2.4 Variation of sensitivity with cutout diameter

as both transducers in a pair did not indicate similar strains (the transducer whose strain increased under the load would produce 60 - 80 percent of the total strain change, depending on the load). This is most likely due to unequal extension/reduction of the wire on either side of the block. The pairs did behave linearly with maximum deviations from linearity between 2 and 5 percent over the range tested.

2.2 System Test Results

The cell was assembled by passing the six wires through the resolver, pre-tensioning them and then clamping them to the resolver. The system was tested by applying forces in the z direction and moments in the y direction with deadweights. Figure 2.5 shows the results when a force F_z is applied, indicating an accuracy of 3.6 percent full scale. For the application of a moment (Figure 2.6), the accuracy is 4.5 percent full scale.

The instrument's ability to resolve forces was also investigated. Figure 2.7 shows the indicated force cross-talk in the x and y directions when a force is applied in the z direction. The cross-talk is less than 1.9 percent of the applied force. At the maximum applied force of 3 N, the indicated moments due to cross-talk are less than 1 N-mm (Figure 2.8).

As mentioned previously, minimizing the deflection of

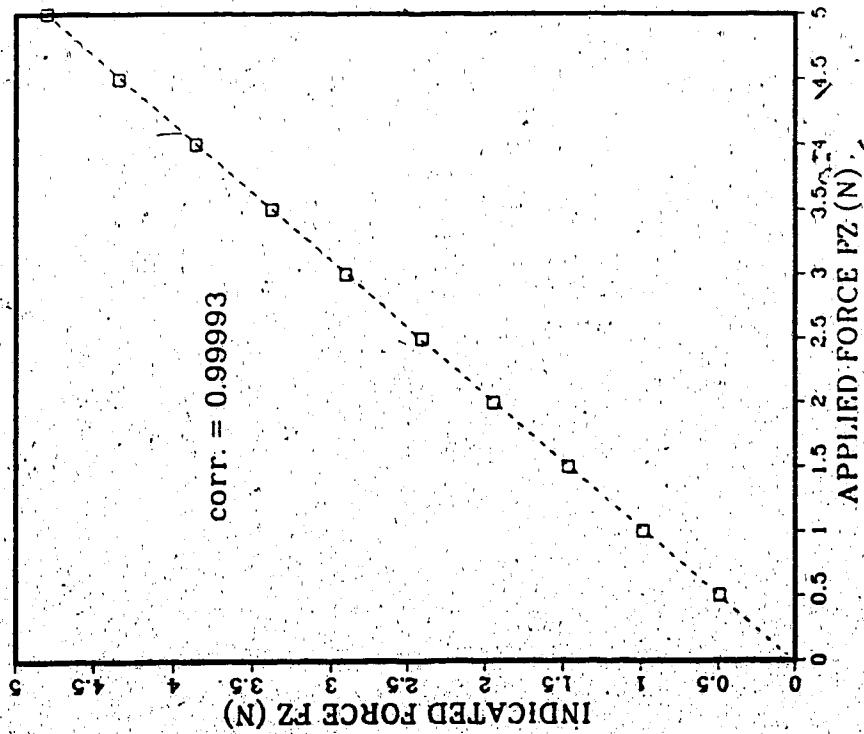


Figure 2.5 Force test results

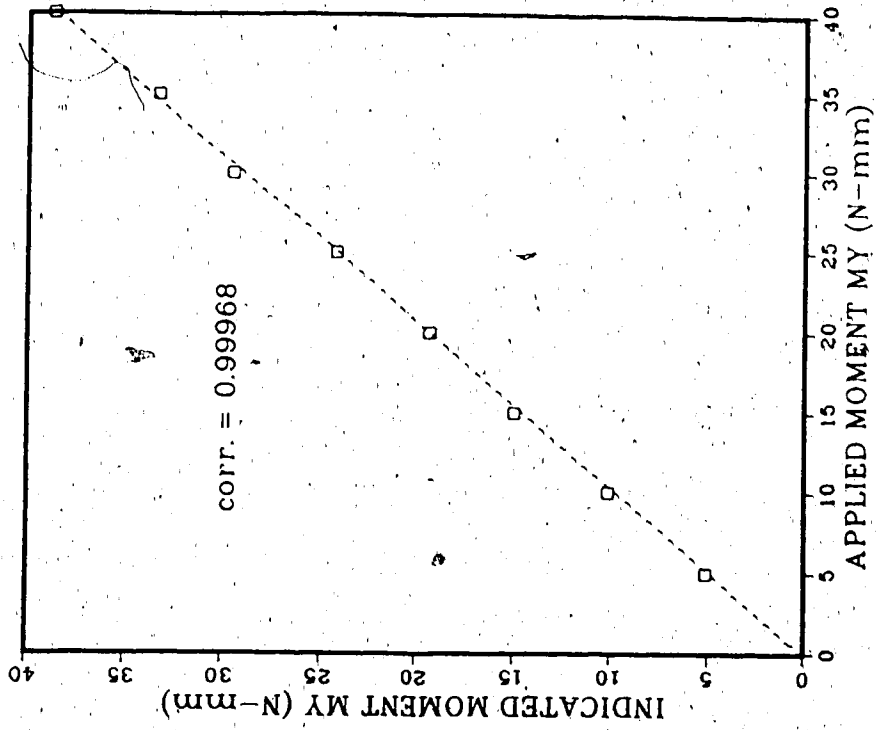


Figure 2.6 Moment test results

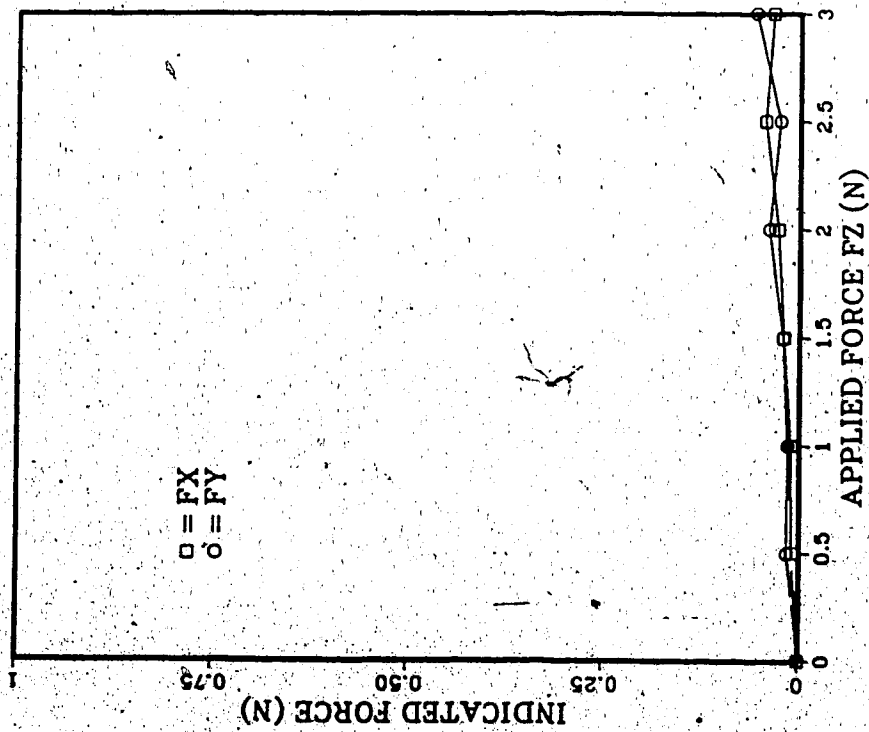


Figure 2.7 Force cross-talk resulting from applied force

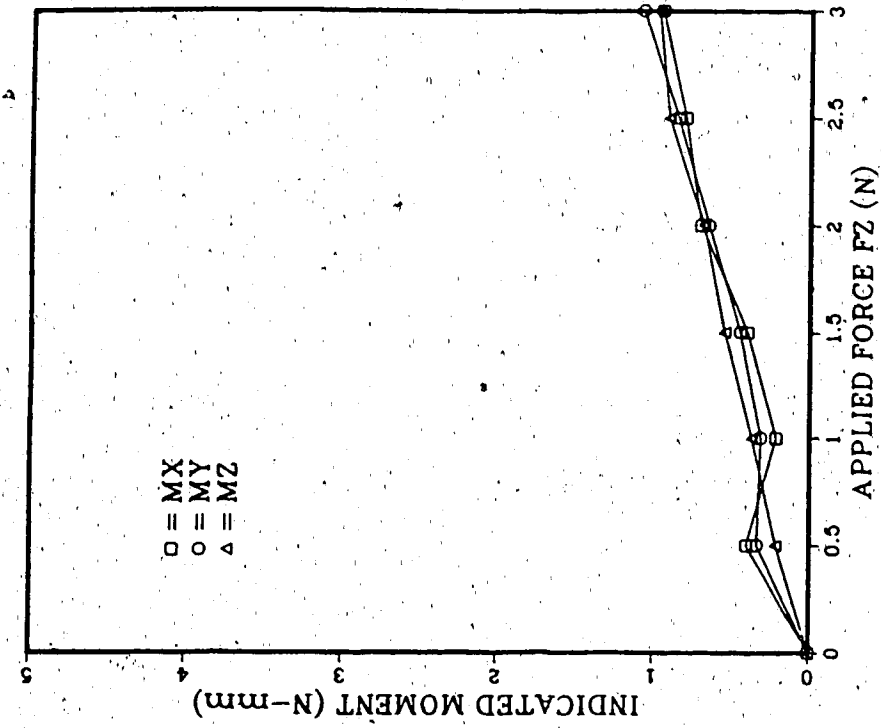


Figure 2.8 Moment cross-talk resulting from applied force

the resolver was a priority. In order to measure the deflection of the resolver under a given force, a depth micrometer was mounted onto the base of the cell and the resolver was displaced in the three coordinate directions while the indicated forces were recorded. The results are shown in Figure 2.9. A force of 5.0 N produces a deflection of 0.09 mm in the z direction. For a stiff orthodontic spring, an activation of 6-8 mm is required to produce a 5 N force. Thus the deflection of the cross resolver is less than 1.5 percent of the activation.

The instrument has been shown to provide adequate performance in its ability to measure forces and moments in the ranges found in orthodontic appliances. The system has displayed an ability to measure forces of up to 5 N with an accuracy of 3.6 percent and moments of 40 N-mm with an accuracy of 4.5 percent. The resolution for forces is 0.003 N in the y direction and 0.005 N in the x and z directions. The corresponding resolutions for moments are 0.06 N-mm and 0.10 N-mm.

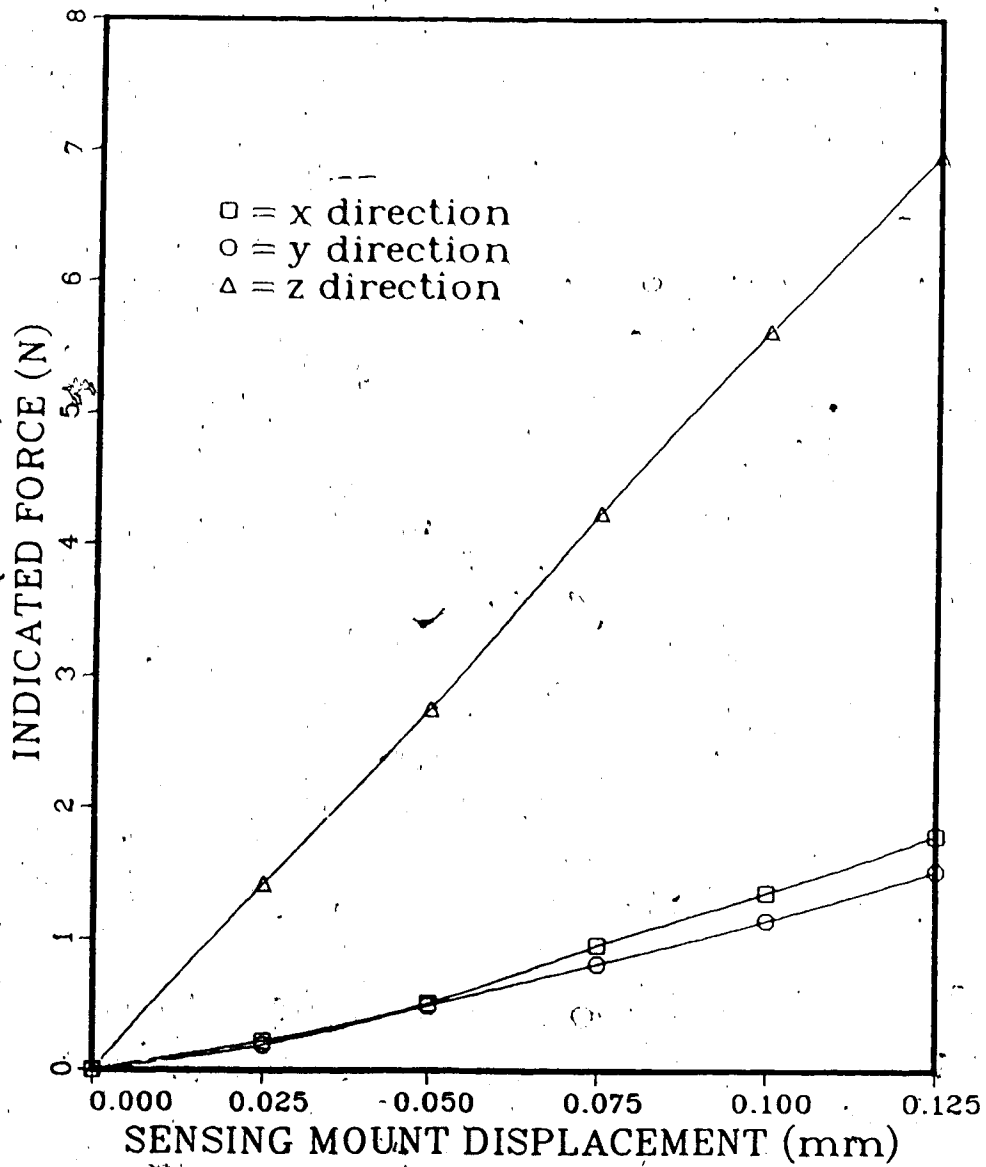


Figure 2.9 Deflection of sensing mount with load

3. FINITE ELEMENT THEORY

The finite element study was conducted using the program ADINA. The appliances were modelled with isoparametric beam elements. Geometrically nonlinear analyses were conducted because of the large displacements and rotations involved. For the springs that were analyzed the strains were assumed to be small and the stress-strain relation was taken to be linear.

3.1 Formulation of Equilibrium Equations

The total Lagrangian incremental formulation is used by ADINA to generate the equations of motion for the isoparametric beam element. The general equations are first produced using the principle of virtual work and then specialized for the particular element. The derivation proceeds as follows.

Consider a body at a time $t+\Delta t$ whose displacement field under a set of external loads t_f corresponding to a time t is known. The displacements at $t+\Delta t$ under the loads $t+\Delta t_f$ are sought therefore the principle of virtual work is written for the body at $t+\Delta t$. The second Piola-Kirchhoff stresses \underline{S} and Lagrange strains \underline{E} are referred to the configuration V_0 of the initial time t_0 . The principle of virtual work is thus

$$\int_{V_0} {}^{t+\Delta t}S_{ij} \delta {}^{t+\Delta t}E_{ij} dV_0 = {}^{t+\Delta t}W_{\text{ext}} \quad (3.1)$$

The stresses and strains are written in terms of increments

$${}^{t+\Delta t}S_{ij} = {}^tS_{ij} + \Delta S_{ij}$$

$${}^{t+\Delta t}E_{ij} = {}^tE_{ij} + \Delta E_{ij}$$

Substituting the following material relation which assumes linearity over the load increment

$$\Delta S_{ij} = C_{ijkl} \Delta E_{kl}$$

and noting that

$$\delta {}^{t+\Delta t}E_{ij} = \delta \Delta E_{ij}$$

gives

$$\int_{V_0} {}^tS_{ij} \delta \Delta E_{ij} dV_0 + \int_{V_0} \Delta E_{kl} C_{ijkl} \delta \Delta E_{ij} dV_0 = {}^{t+\Delta t}W_{\text{ext}} \quad (3.2)$$

It can be shown that

$$\Delta E_{ij} = \frac{1}{2} (\Delta \bar{u}_{i,j} + \Delta \bar{u}_{j,i} + \bar{u}_{k,i} \Delta \bar{u}_{k,j} + \bar{u}_{k,j} \Delta \bar{u}_{k,i} + \Delta \bar{u}_{k,i} \Delta \bar{u}_{k,j})$$

where $\bar{u}_{i,j}$ are the displacement derivatives at t and $\Delta\bar{u}_{i,j}$ are the increment derivatives. The last term applies only for large strains. The increment in Lagrange strains is written as the sum of linear and nonlinear components

$$\Delta E_{ij} = \Delta E_{ij}^l + \Delta E_{ij}^{nl}$$

Substituting into (3.2) and making a further linearizing assumption by neglecting the product of the stress increment and nonlinear strain increment in the second term gives

$$\int_{V_0} {}^t S_{ij} \delta(\Delta E_{ij}^l + \Delta E_{ij}^{nl}) + \int_{V_0} \Delta E_{kl}^l C_{ijkl} \delta \Delta E_{ij}^l dV_0 = {}^{t+\Delta t} W_{\text{ext}} \quad (3.3)$$

The external virtual work is given by

$${}^{t+\Delta t} W_{\text{ext}} = \int_{V_0} {}^{t+\Delta t} f_b \delta u_i dV_0 + \int_{S_0} {}^{t+\Delta t} f_s \delta u_i dS_0 \quad (3.4)$$

where f_b and f_s denote body forces and surface tractions.

Discretizing the equation by using the following interpolations for the displacements and strains in terms

of the nodal displacements

$$\Delta \bar{u} = \underline{H} \Delta u \quad (3.5)$$

$$\Delta E^1 = \underline{B} \Delta u \quad (3.6)$$

and invoking the principle of virtual work results in the matrix equation

$$\begin{aligned} & \left[\int_{V_0} \underline{t}_B^T \underline{C}^T \underline{B} \, dV_0 + \int_{V_0} \underline{t}_H^T \underline{S} \underline{H}' \, dV_0 \right] \Delta \bar{u} \\ & = \int_{V_0} \underline{t}^{t+\Delta t}_{f_b} \delta u_i \, dV_0 + \int_{S_0} \underline{t}^{t+\Delta t}_{f_s} \delta u_i \, dS_0 + \int_{V_0} \underline{t}_B^T \underline{S} \, dV_0 \end{aligned}$$

$$\text{or} \quad (\underline{t}_K^1 + \underline{t}_K^{nl}) \Delta u = \underline{t}^{t+\Delta t}_R - \underline{t}^{t+\Delta t}_F \quad (3.7)$$

where

$\underline{t}_K^1, \underline{t}_K^{nl}$ = linear and initial stress incremental stiffness matrices

Δu = vector of increments in the nodal displacements

$\underline{t}^{t+\Delta t}_R$ = vector of externally applied nodal loads at $t+\Delta t$

$\underline{t}^{t+\Delta t}_F$ = vector of nodal point forces equivalent to the integration of internal stresses

The updated Lagrangian incremental formulation is similar to the total Lagrangian formulation except that the

stresses and strains are referred to an updated configuration; namely the configuration at time t . The elements are usually formulated with respect to the local element coordinate system. The calculation of the strain-displacement relation (3.6) requires the transformation from the global to the local coordinate system. In the TLF this transformation does not change because the original configuration is taken as the reference configuration, which does not change. In the ULF the transformation must be updated with each step. When second Piola-Kirchhoff stresses and Lagrange strains (which are invariant under rigid body rotation) are used, the TLF and ULF are theoretically equivalent as the rigid body rotations of the local element coordinate systems are accounted for in the TLF.

3.2 Solution Strategy

The solution for the displacement increments must necessarily be iterative as t_{K}^{nl} and $t+\Delta t_F$ are dependent on the displacement field. The most straight-forward procedure is the modified Newton-Raphson iteration

$$t_{K} \Delta u(i) = t+\Delta t_R - t+\Delta t_F(i-1)$$

$$t+\Delta t_u(i) = t+\Delta t_u(i-1) + \Delta u(i)$$

The convergence is illustrated schematically for a scalar problem in Figure 3.1. The tangent stiffness at time t is used throughout the process. The curve represents the nodal loads which have been found by integrating the stress field obtained from a strain field corresponding to the nodal displacement. In standard Newton-Raphson iteration the tangent stiffness at the end of each iteration is used, and the formation of the stiffness matrix with each iteration can become costly. A more economical iterative process is the BFGS (Broyden-Fanno-Goldfarb-Schmidt) method which was used for this analysis. The equation used is

$${}^{t+\Delta t}K^*(i-1)\Delta u(i) = {}^{t+\Delta t}R - {}^{t+\Delta t}F(i-1) \quad (3.8)$$

${}^{t+\Delta t}K^*(i-1)$ is a stiffness matrix which is updated in iteration i to satisfy the secant relation

$${}^{t+\Delta t}K^*(i) [{}^{t+\Delta t}u(i) - {}^{t+\Delta t}u(i-1)] = [{}^{t+\Delta t}R - {}^{t+\Delta t}F(i)] - [{}^{t+\Delta t}R - {}^{t+\Delta t}F(i-1)]$$

In addition, the displacement vector update is optimized through the use of a scalar acceleration factor

$${}^{t+\Delta t}u(i) = {}^{t+\Delta t}u(i-1) + \eta(i) \Delta u(i)$$

The multiplier η is obtained by minimizing the quantity

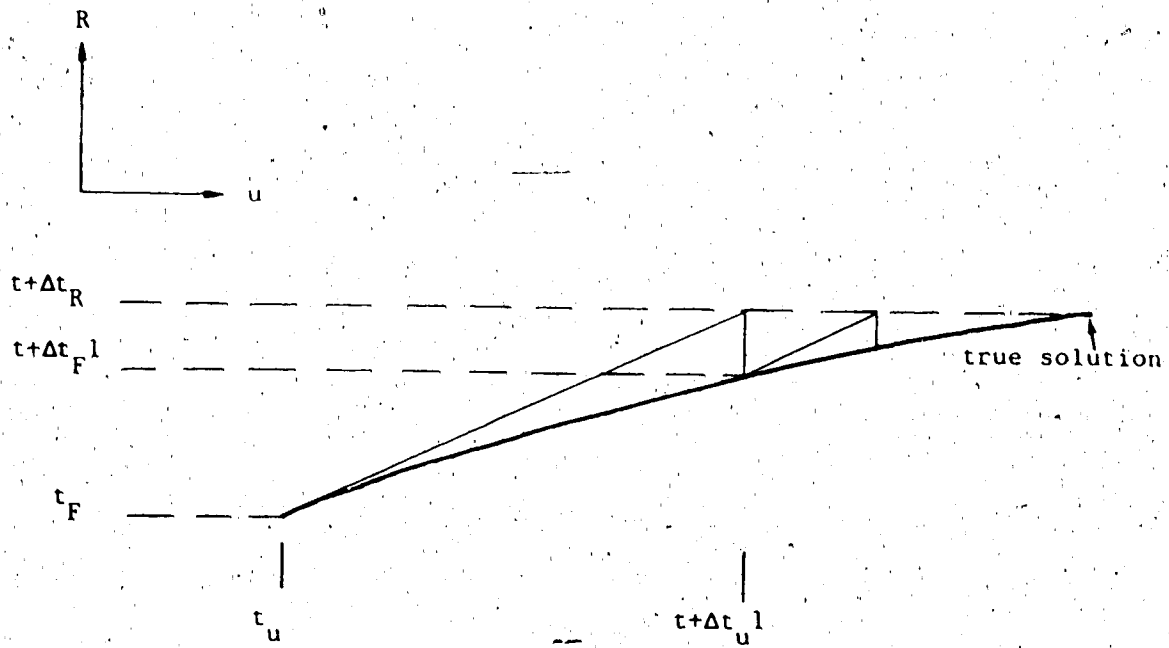


Figure 3.1 Modified Newton-Raphson iterative solution for increment in displacements

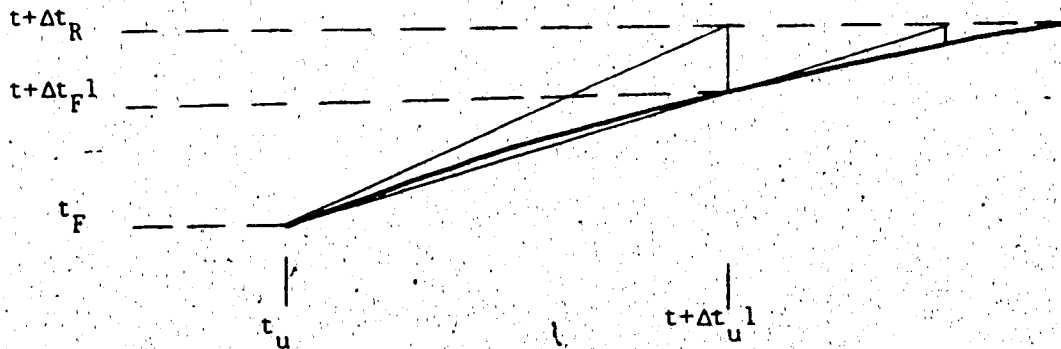


Figure 3.2 BFGS solution

$$\Delta u(i)T (t+\Delta t_R - t+\Delta t_F(i))$$

The convergence process is illustrated in Figure 3.2.

3.3 Convergence Criteria

Convergence is considered attained when both the force and energy criteria are satisfied. The force criterion for iteration i is that the Euclidean norm of the out-of-balance vector be less than a specified force tolerance (Figure 3.2)

$$\| t+\Delta t_R - t+\Delta t_F(i-1) \| < \text{force tolerance}$$

The energy criterion for iteration i is that the ratio of the out-of-balance work to the external work during the load increment be less than a specified tolerance

$$\frac{\Delta u(i)T (t+\Delta t_R - t+\Delta t_F(i-1))}{\Delta u(i)T (t+\Delta t_R - t_F)} < \text{energy tolerance}$$

3.4 Isoparametric Beam Element

The basic interpolations used in the calculation of the element matrices of the three-dimensional isoparametric beam element are now presented. In the coordinate and

displacement interpolations plane rectangular cross-sections of the beam normal to the neutral axis are assumed to remain plane although not necessarily normal to the axis. Therefore this element should not be used for torsion problems but the effects of shear deformation are included.

The geometry of the element at time t is given by

$$t_x(r,s,t) = \sum_k h_k t_{x_k} + \frac{t}{2} \sum_k a_k h_k v_{tx}^k + \frac{s}{2} \sum_k b_k h_k v_{sx}^k$$

$$t_y(r,s,t) = \sum_k h_k t_{y_k} + \frac{t}{2} \sum_k a_k h_k v_{ty}^k + \frac{s}{2} \sum_k b_k h_k v_{sy}^k$$

$$t_z(r,s,t) = \sum_k h_k t_{z_k} + \frac{t}{2} \sum_k a_k h_k v_{tz}^k + \frac{s}{2} \sum_k b_k h_k v_{sz}^k$$

where

(3.9)

r, s, t are the local coordinates

$h_k(r)$ are the one-dimensional interpolation functions

x_k, y_k, z_k are the global coordinates for node k

a_k, b_k are the cross-sectional dimensions

$v_{tx}^k, v_{ty}^k, v_{tz}^k$ are the components of the unit vector V_{tk} in the direction t at node k

$v_{sx}^k, v_{sy}^k, v_{sz}^k$ are the components of the unit vector V_{sk} in the direction s at node k

The coordinate systems and vectors are shown in Figure 3.3. A schematic diagram illustrating this coordinate interpolation is shown in Figure 3.4. The figure shows a two-node element in the r - t plane. Considering the point $(r,s,t) = (0,0,1)$, the x coordinate of the point is given using linear interpolation functions as

$$\begin{aligned} x(0,0,1) &= 0.5(1-r_1)x_1 + 0.5(1+r_2)x_2 \\ &+ t [0.5a_1(1-r_1)v_{tx}^1 + 0.5a_2(1+r_2)v_{tx}^2] \\ &= 0.5(x_1 + x_2 + 0.5[a_1v_{tx}^1 + a_2v_{tx}^2]) \end{aligned}$$

The displacement components at time t and the incremental displacement components are given by

$$t u_i = t x_i - o x_i \quad \text{and} \quad u_i = t+\Delta t x_i - t x_i$$

Substituting the geometry interpolations yields expressions for the displacement components in terms of the nodal displacements and differences in the direction cosines of the nodal vectors

$$t u_i = \sum_k h_k t u_i^k + \frac{t}{2} \sum_k a_k h_k (t v_{ti}^k - o v_{ti}^k)$$

$$\frac{t}{2} \sum_k b_k h_k (t v_{si}^k - o v_{si}^k)$$

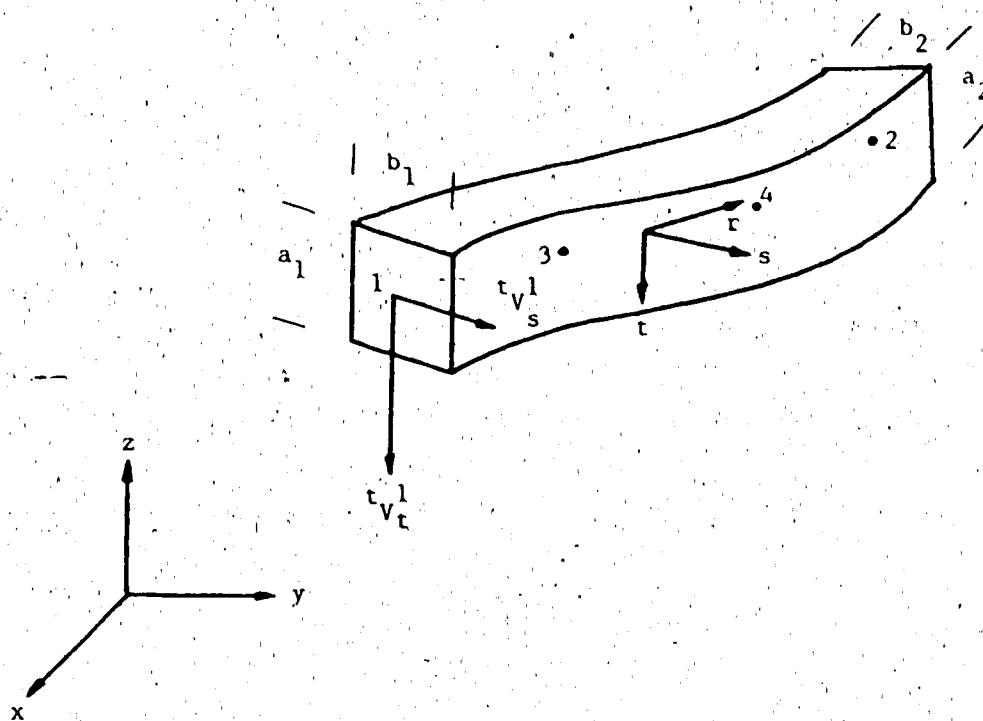


Figure 3.3 Coordinate systems and position vectors for isoparametric beam element

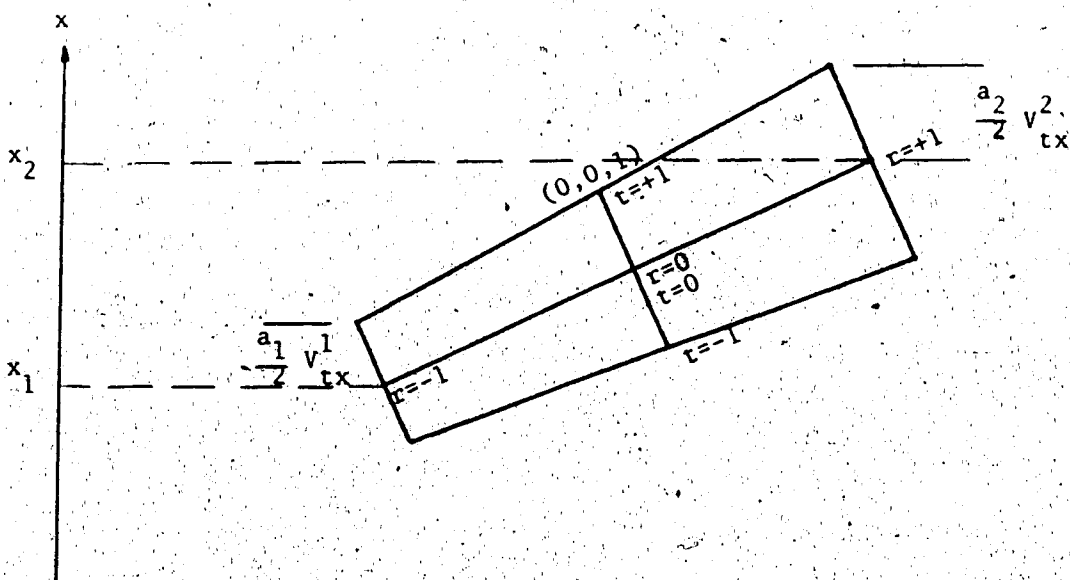


Figure 3.4 Two-dimensional, two-node illustration of coordinate interpolations

$$u_i = \sum_k h_k u_i^k + \frac{t}{2} \sum_k a_k h_k \Delta v_{ti}^k + \frac{s}{2} \sum_k b_k h_k \Delta v_{si}^k$$

where

$$\Delta v_{ti}^k = t + \Delta t v_{ti}^k - t v_{ti}^k$$

$$\Delta v_{si}^k = t + \Delta t v_{si}^k - t v_{si}^k$$

It is desired to express the displacements in terms of the nodal displacements and rotations. The difference vectors Δv_{ti}^k and Δv_{si}^k are therefore written in terms of rotations about the global axes

$$\Delta v_t^k = \theta_k \times t v_t^k$$

$$\Delta v_s^k = \theta_k \times t v_s^k$$

These relations are accurate providing that the rotations are small. In order to allow for large rotations the directions of the new nodal vectors are calculated as

$$t + \Delta t v_t^k = t v_t^k + \int \frac{d\theta_k}{\theta_k} \times t v_t^k$$

$$t + \Delta t v_s^k = t v_s^k + \int \frac{d\theta_k}{\theta_k} \times t v_s^k$$

These relations are the basic interpolations used to

evaluate the strain-displacement interpolation matrices for the incremental formulation. The calculation of the necessary matrices is described in [20].

4. TEST RESULTS

In this chapter the details and results of the numerical and experimental studies that were done are given. Two studies were completed to obtain a comparison between numerical and experimental results. Further experimental studies were carried out to investigate the effects of varying certain geometrical parameters on T springs, to obtain further insight into the behaviour of these appliances.

4.1 Comparative Studies

Case 1

The first spring to be studied was the non-preactivated spring of Figure 4.1. This appliance had been tested and modelled previously by Koenig et al. [8].

The spring was bent from .010 x .020 in. (.25 x .51mm) stainless steel wire. The values for Young's modulus and Poisson's ratio for the material were assumed to be 177 GPa and 0.30 [22]. All springs were made using pliers and matched templates to within 0.25 mm. Visual inspection revealed the out-of-plane error to be less than 0.5 mm. The spring was clamped at an interbracket distance of 7 mm and the ends were displaced in the -z direction to an interbracket distance of 9 mm. The test was carried out

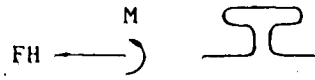


Figure 4.1 T spring with no pre-activation

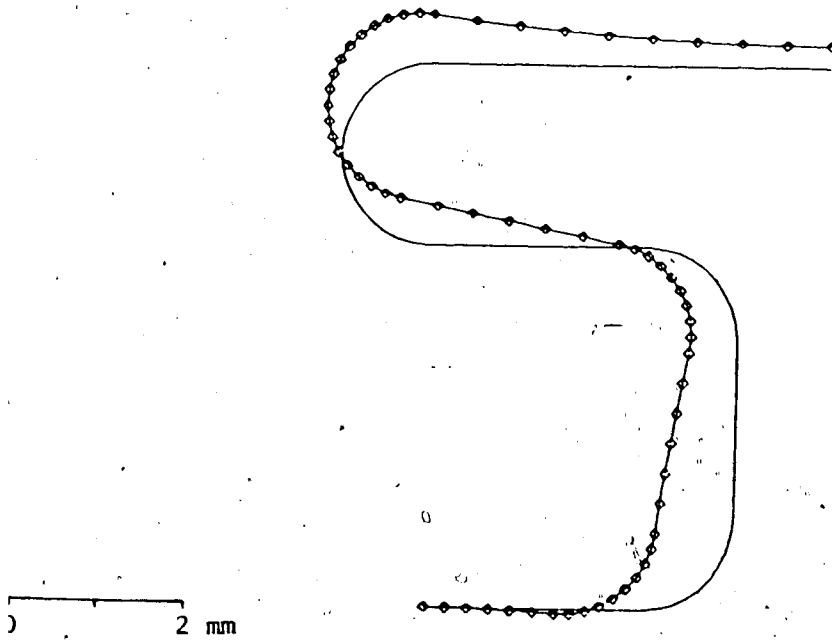


Figure 4.2 Original and deformed finite element mesh

using the same spring four times.

The finite element mesh is shown in Figure 4.2. Because of symmetry only half the spring was modelled. Four-node isoparametric beam elements were used. The boundary conditions used specified no rotation and no vertical translation at the clamped end and no rotation and no horizontal translation at the midplane end. In order to obtain a measure of the convergence towards the actual force-deflection relationship the program was run using meshes consisting of 21 and 26 elements. A linear analysis was followed by a geometrically nonlinear analysis with the displacement applied in eight increments. BFGS iteration was used until the ratio of out-of-balance energy to incremental energy fell below 0.001. When equilibrium was checked using the forces and moments at either end of the half-spring the out-of-balance forces were found to be less than 0.007 N and the out-of-balance moments were less than 0.10 N-mm.

Figures 4.3 and 4.4 are summaries of the force-deflection and moment-deflection relationships that were calculated and measured. All experimental results are tabulated in the appendix. The standard deviations of the force and moment data fell below 2.5 and 3.1 percent respectively. The calculated values obtained using the 26 element model differed from the results obtained using the coarser model by less than 1 percent. The calculated and measured curves given by Koenig et al. [8]

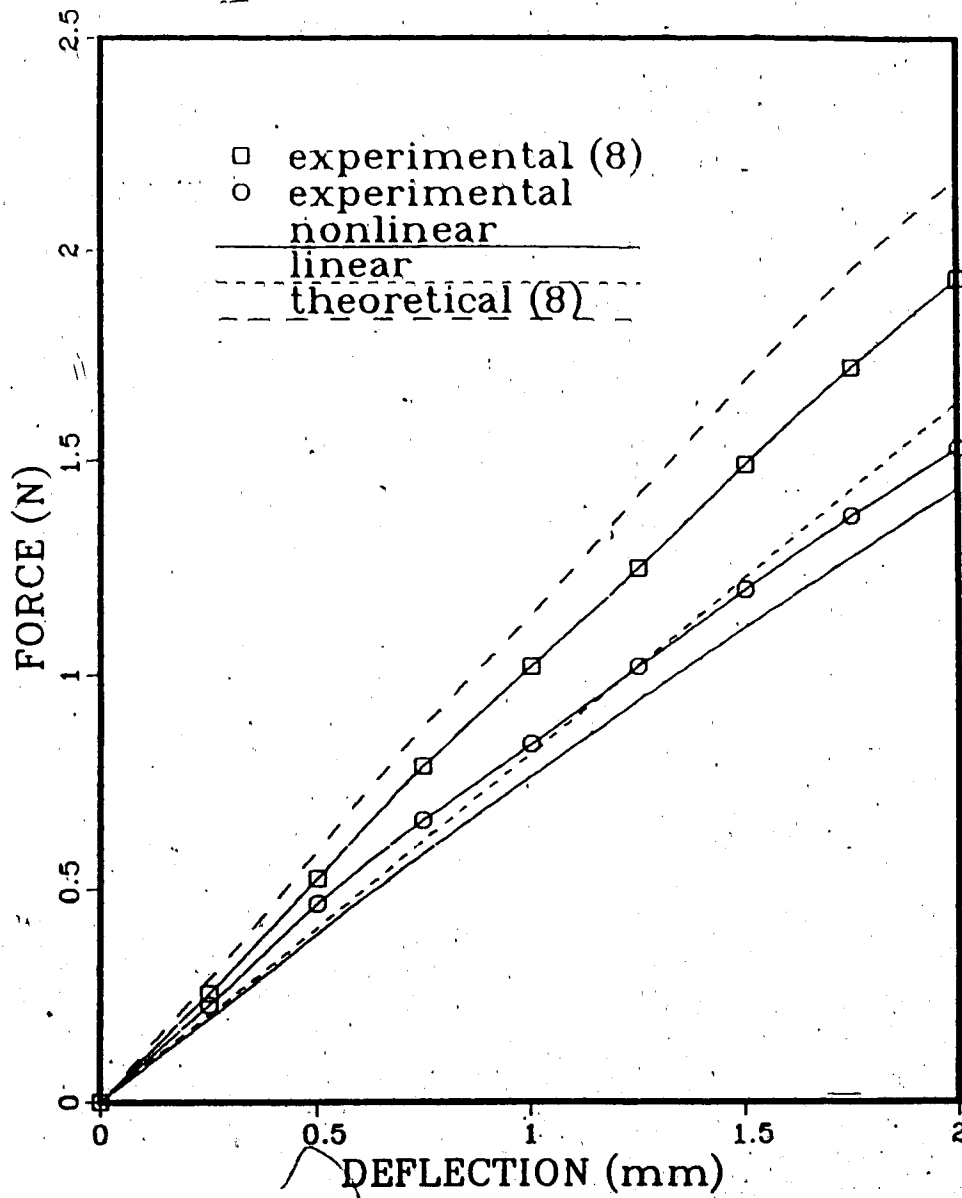


Figure 4.3 Force-deflection relationships

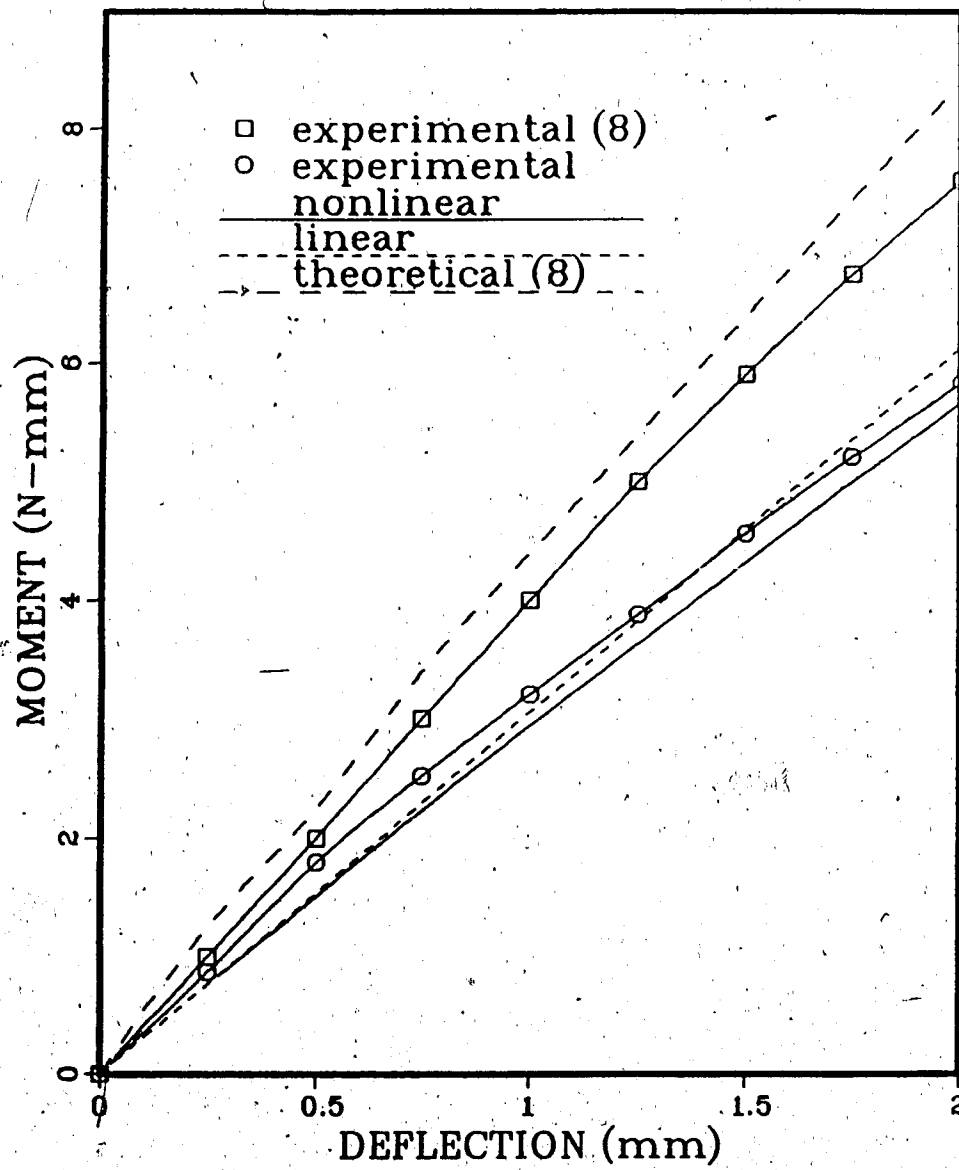


Figure 4.4 Moment-deflection relationships

are also shown. The results show good agreement between the calculated and measured values considering the variations possible in constructing and mounting the spring. Differences in the stainless steel wire could account for some of the differences between the previous study and these results.

Case 2

An experimental and theoretical comparison was also performed for the pre-activated spring of Figure 4.5. The spring was bent from .017 x .025 in. (.43 x .64 mm) TMA wire. The values for Young's modulus and Poisson's ratio were taken to be 69 GPa and 0.31 [23].

The spring was clamped at an interbracket distance of 19 mm, deformed into the neutral position (at the neutral position both ends of the spring have the same slope and the spring experiences a pure bending moment) and then activated in the -z direction to increase the interbracket distance by 7 mm. The prescribed end rotation and displacement applied to the finite element model are shown in Figure 4.6. The program was run up to the neutral position to calculate the end displacement, which was found to be 5.89 mm. It was then restarted and the prescribed displacement of -3.5 mm was applied.

The complete loading was applied in 160 increments as this resulted in the most economical solution to satisfy

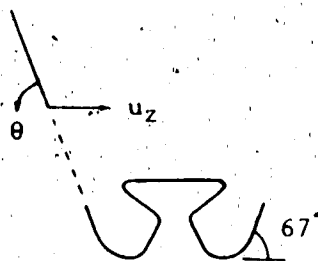


Figure 4.5 Pre-activated T spring

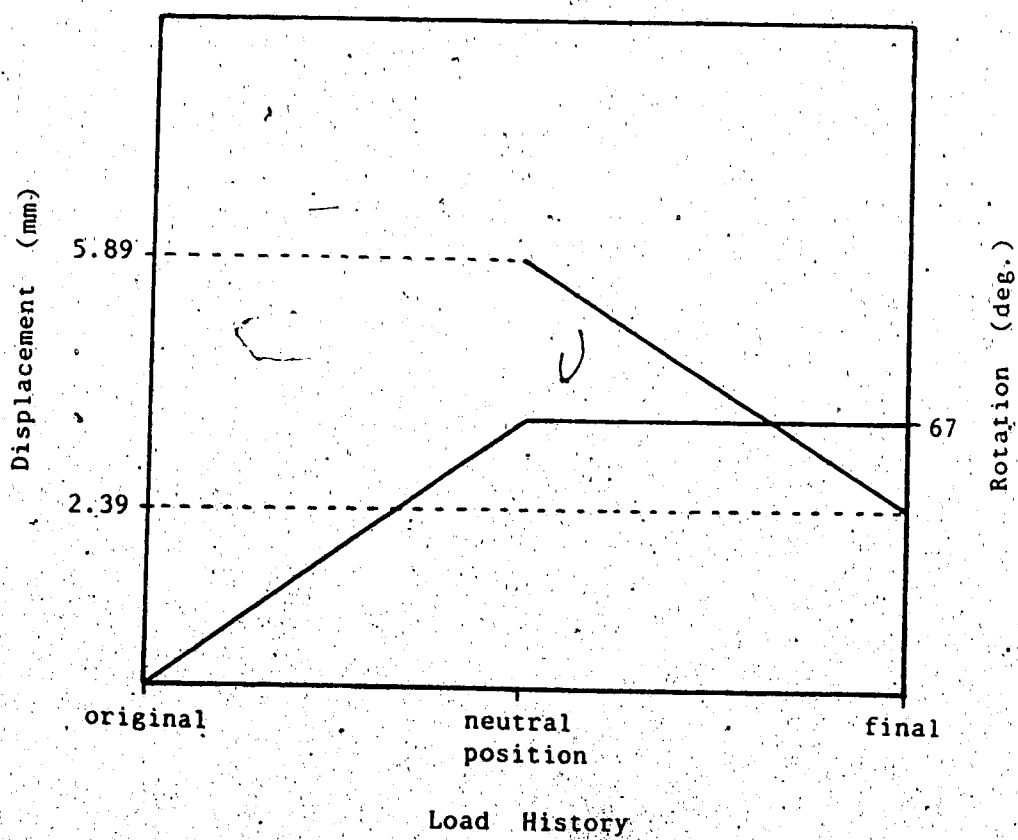


Figure 4.6 Prescribed rotation and displacement of spring end

the convergence requirements. The convergence difficulties with this problem were a result of nonlinear effects in the spring stiffness due to the large displacements and rotations involved. Relaxing the convergence tolerance was not a suitable alternative as it resulted in fluctuations in the numerically small axial end force. Approximately one third of the solution time was spent in updating the inverse of the stiffness matrix and the remainder was spent on equilibrium iterations.

The finite element mesh is shown in Figure 4.7. The model was restrained from vertical translation at the clamped end and restrained from rotation and horizontal translation at the midplane end. The model contained 26 four node beam elements. BFGS iteration was used until the Euclidean norm of the out of balance load vector fell below 0.01 N. This resulted in out-of-balance forces of less than 0.002 N and out-of-balance moments of less than 0.08 N-mm for the model.

The calculated end displacement at the neutral position was 5.89 mm (Figure 4.6). The displacement was measured to be 5.7 mm. The calculated and measured forces and moments versus deflection from the neutral position are shown in Figures 4.8,9. The model over-estimated the maximum force by 15 percent and the maximum moment by 8 percent. Inaccuracies in the assumed material properties may be partially responsible for these differences.

Finally, a linear analysis was also performed. The

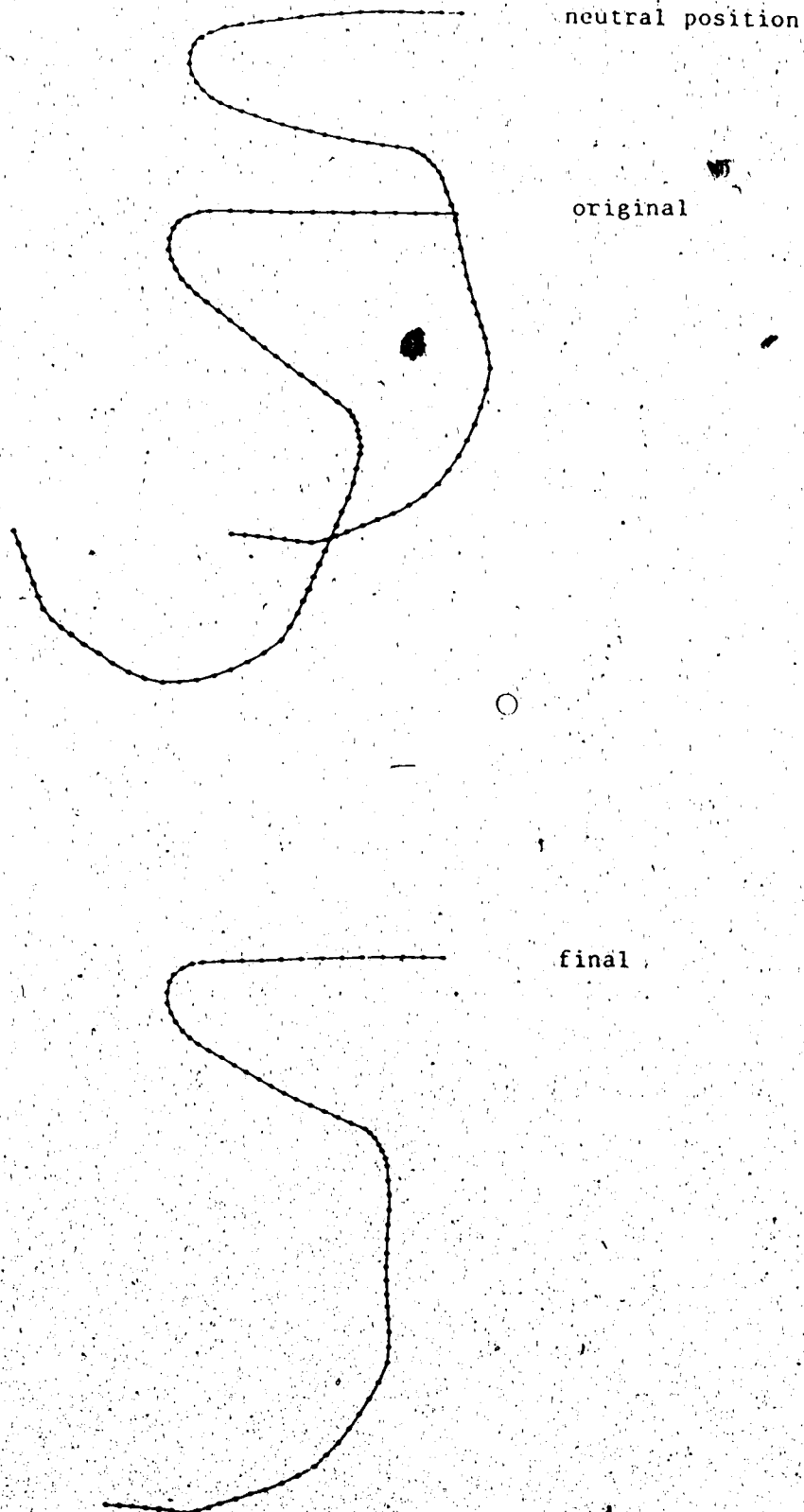


Figure 4.7 Finite element mesh

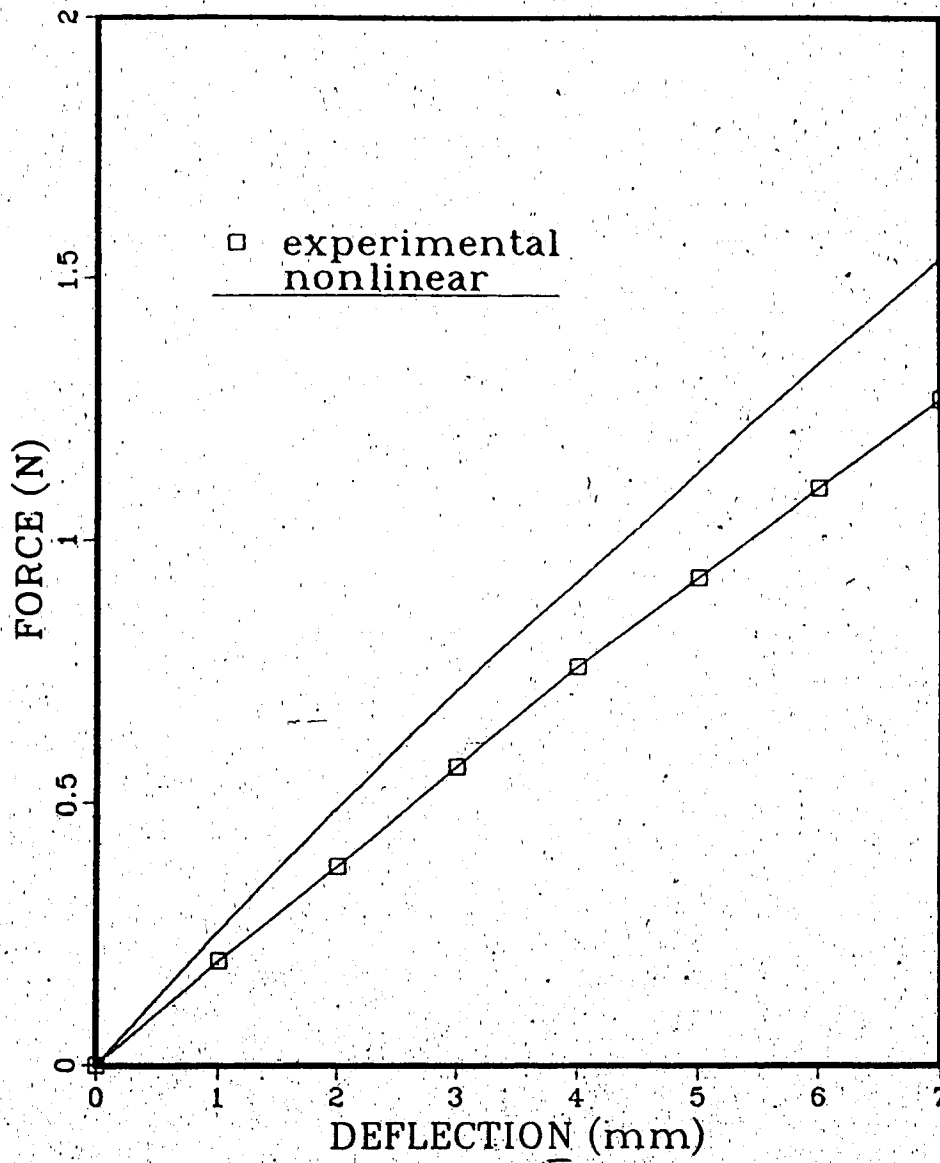


Figure 4.8 Force vs. deflection from neutral position

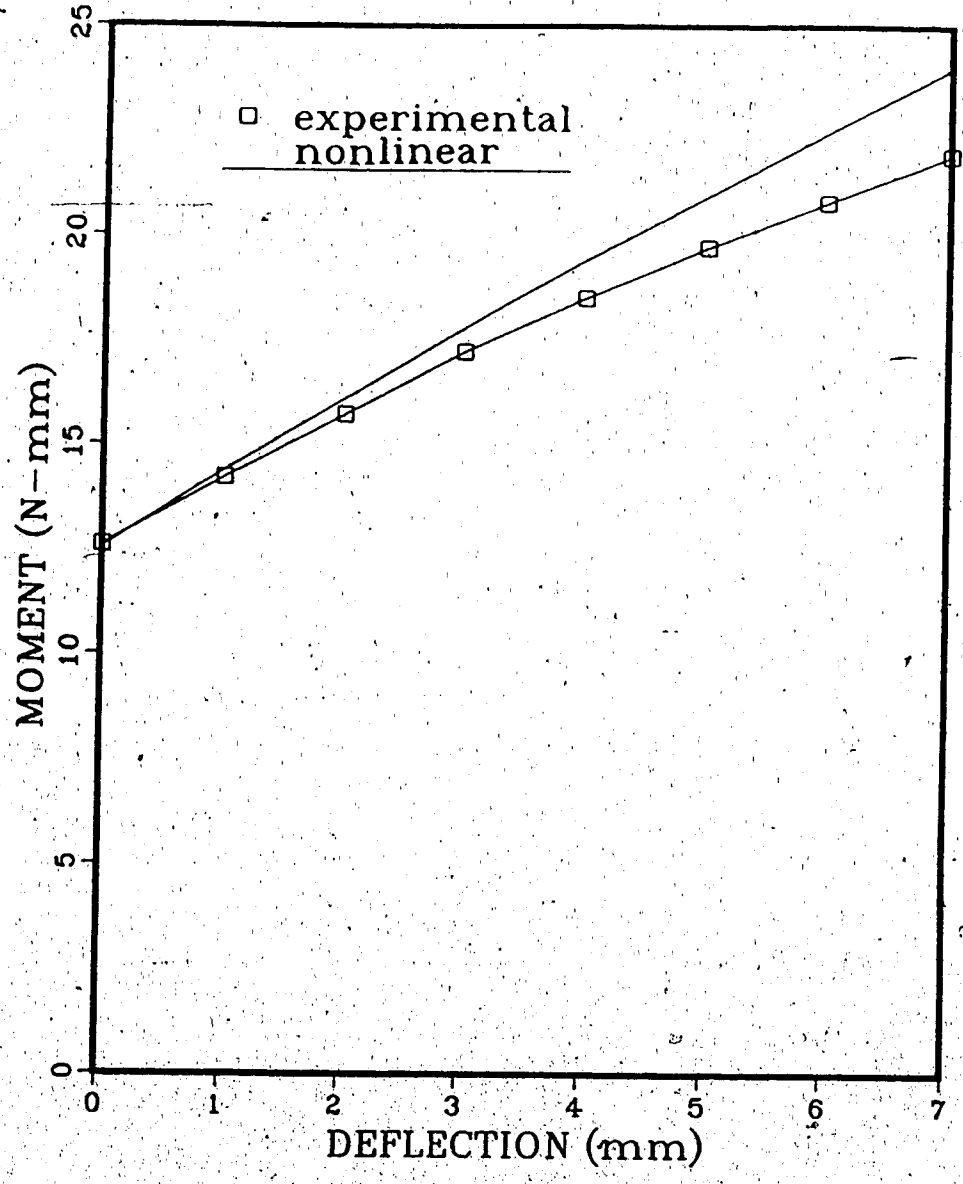


Figure 4.9 Moment vs. deflection from neutral position

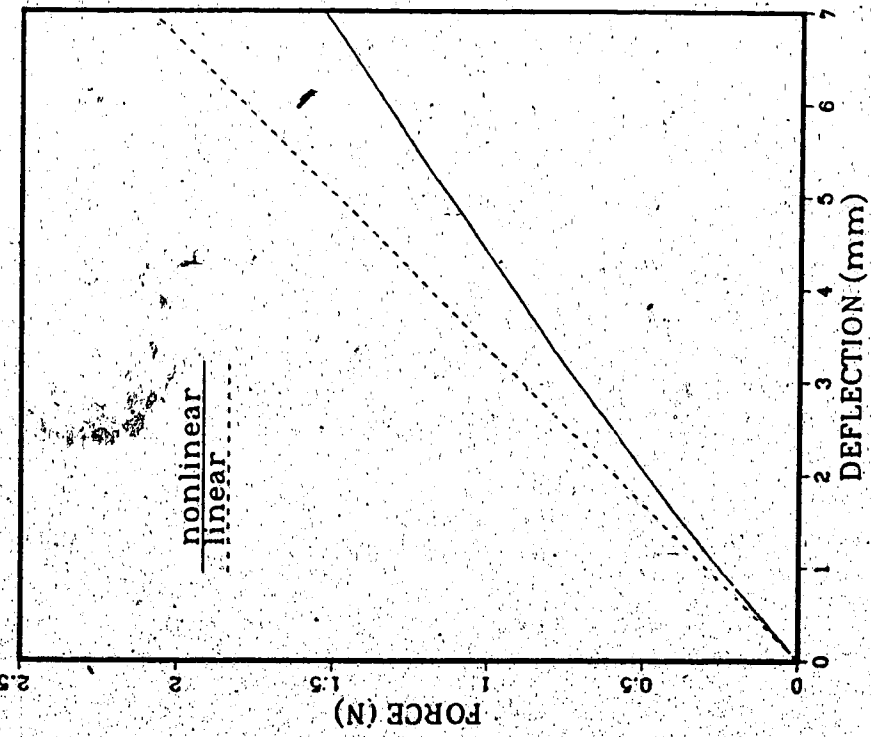


Fig. 4.10 Calculated force-deflection relationships

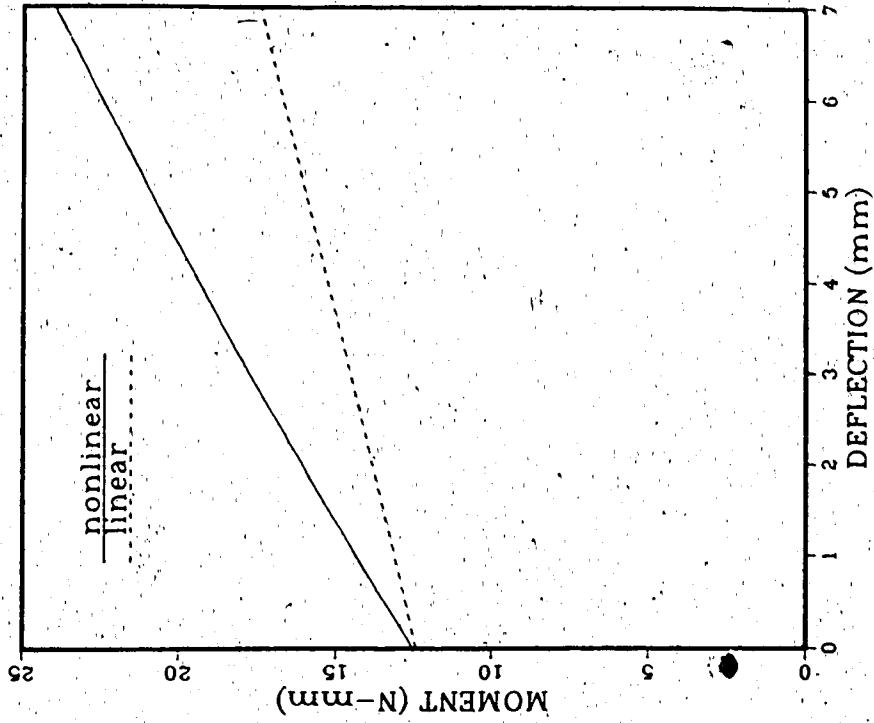


Fig. 4.11 Calculated moment-deflection relationships

calculated linear and nonlinear forces and moments are shown in Figures 4.10,11. Due to the large displacements and rotations involved, poor agreement was seen between the linear and nonlinear results. The values for the moment at the neutral position however, differ by only 1 percent (the moment-rotation relation to the neutral position that was calculated with the nonlinear analysis was found to depart from linearity by less than 1 percent). The calculated end displacement at the neutral position however, was 2.76 mm compared to 5.89 mm for the nonlinear analysis.

4.2 Parametric Studies

The geometric parameters that were varied were spring height, activation angle, centering between brackets and the addition of helices. All of the appliances that were tested were constructed from 0.017 x 0.025 in. TMA wire.

Case 1

This study investigated the effect of spring height. Four springs of 5, 6, 7 and 8 mm non-preactivated height were tested. The springs are shown in Figure 4.12.

Each spring was clamped at a distance of 2 mm from the activation bends nearest the ends, deformed into the neutral position and then activated to increase the

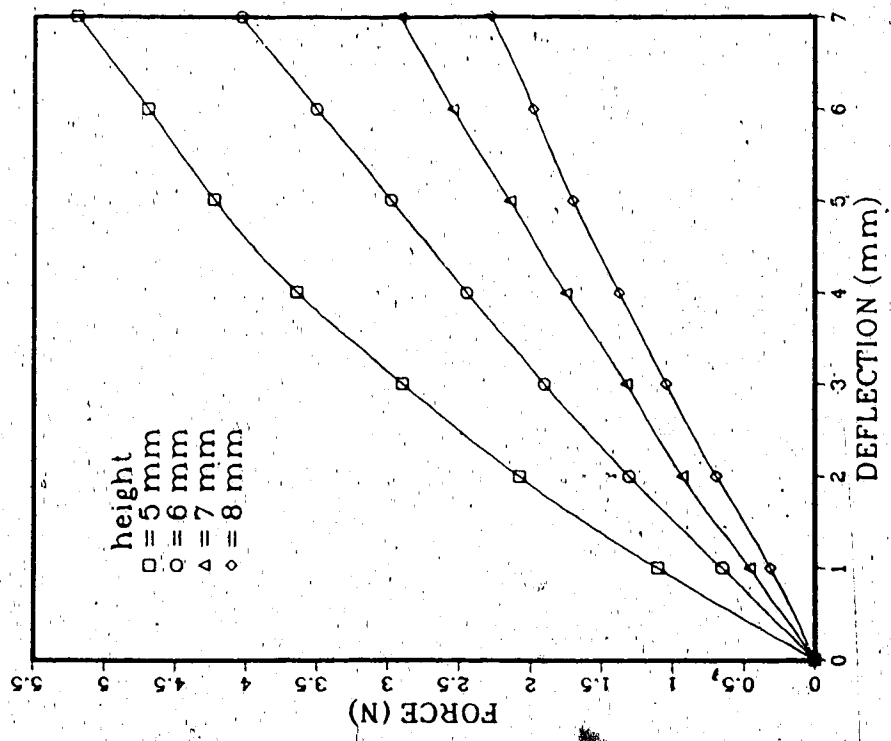
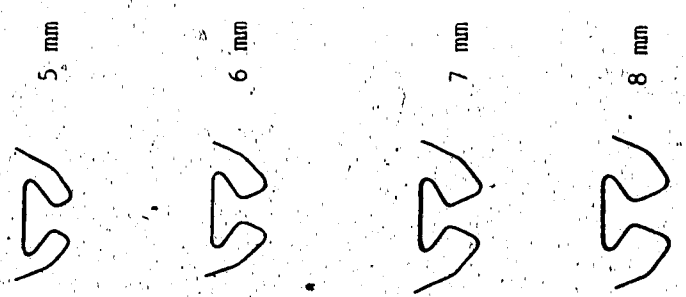


Fig. 4.12 Spring height variation

Fig. 4.13 Force-deflection relationship

interbracket distance by 7 mm. Four tests were conducted for each spring. The neutral position of each spring was determined by varying the interbracket distance so that the forces were close to zero. The interbracket distances at the neutral position were found to be 10.5, 11.5, 12.0 and 12.5 mm in order of increasing spring height.

Figures 4.13, 4.14 and 4.15 show the horizontal force, moment and moment to force ratio versus deflection from the neutral position. The results indicate a larger increase in force delivery than moment with decreasing spring height. At an activation of 4 mm the force delivered by the 5 mm spring was 2.8 times as large as the force exerted by the 8 mm spring. The corresponding increase in moment was 30 percent, consequently the moment to force ratio varies considerably with spring height. Finally, the abrupt change in slope of the force and moment curves for the 5 mm spring indicates that the spring yielded at a deflection from the neutral position of between 4 and 5 mm.

Case 2

The effect of varying the activation angles was also studied. Four springs based on the 8 mm spring of the previous study were constructed. The springs are shown in Figure 4.16. The α and β angles, originally at 30° were changed as follows: α was increased by 30° ; α was increased by 60° ; α was increased by 30° and β was decreased by 30° ;

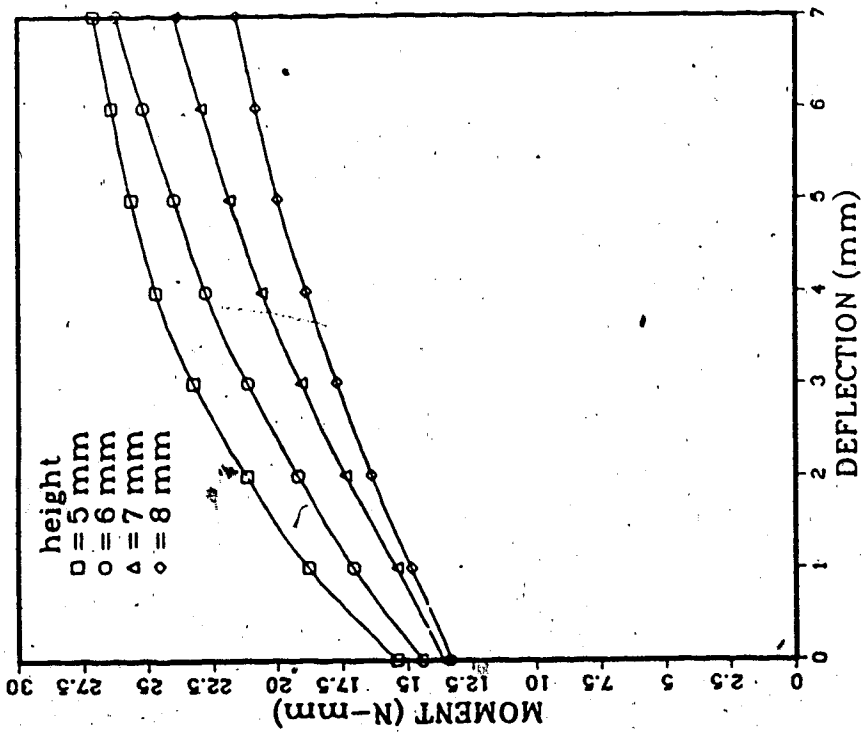


Fig. 4.14 Moment-deflection relationship

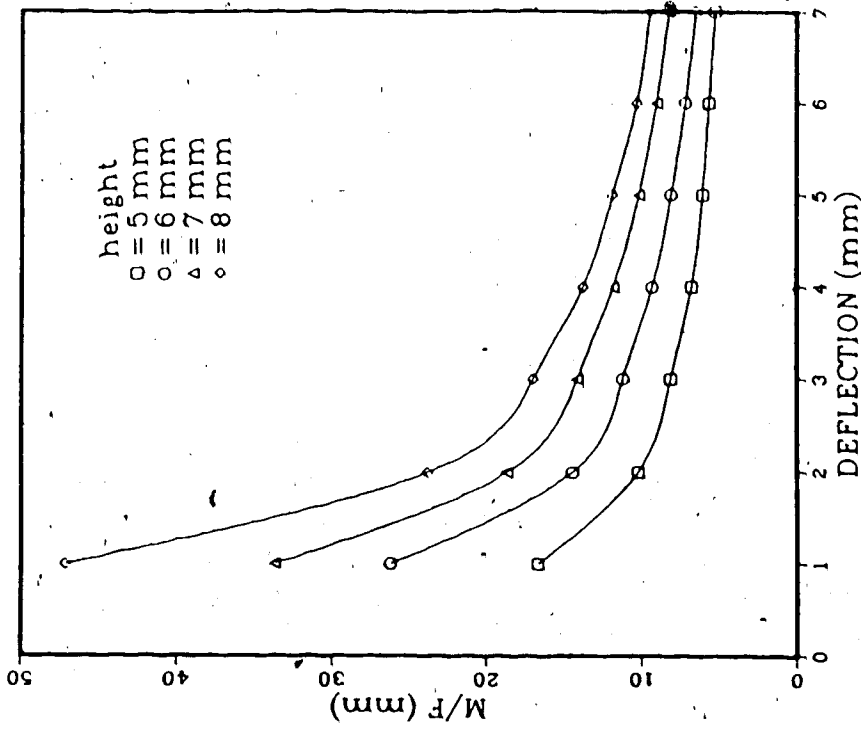


Fig. 4.15 Moment to force ratio vs. deflection from neutral position

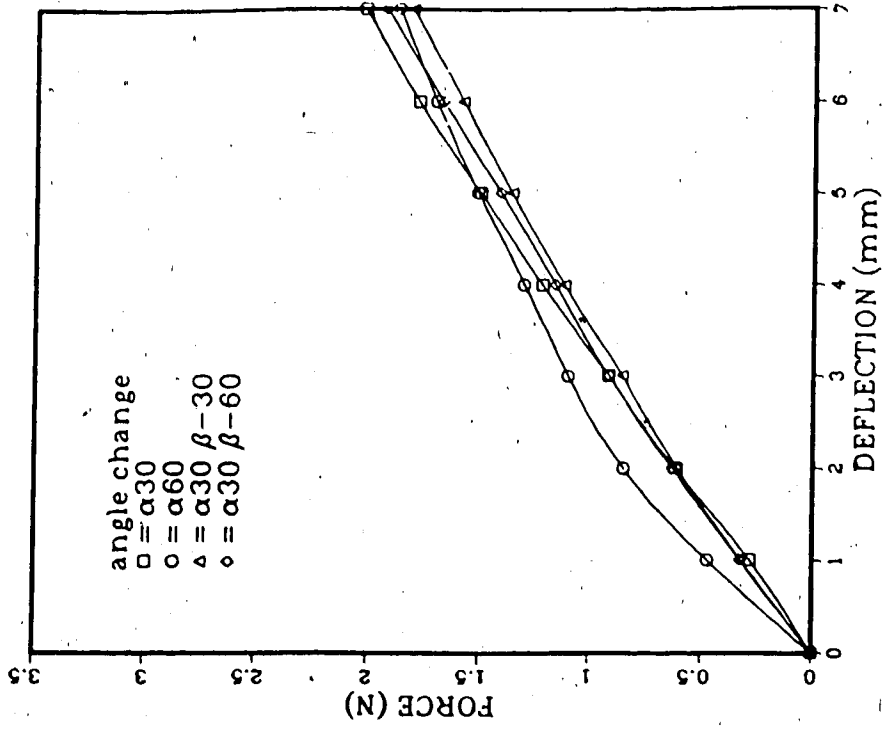
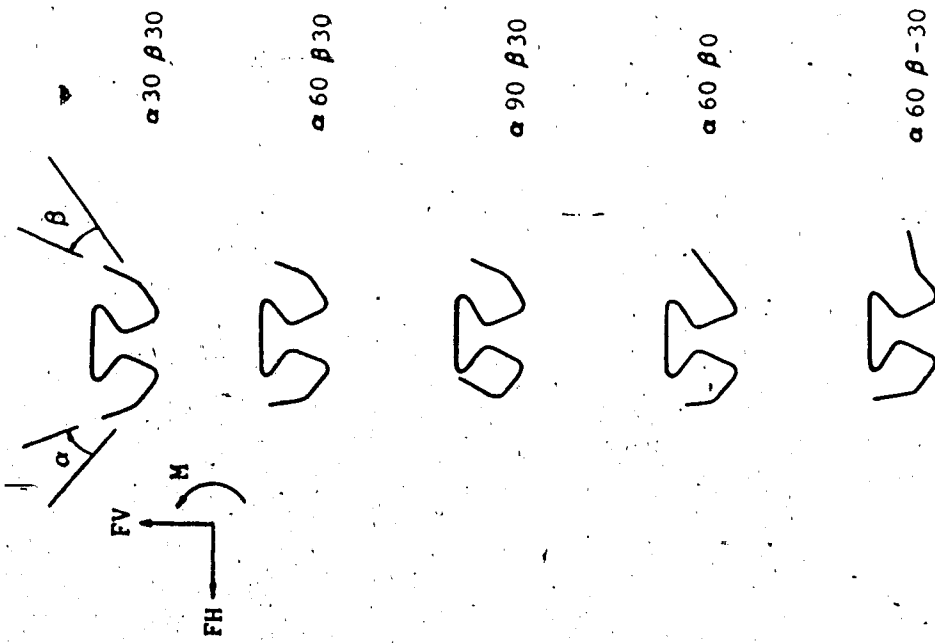


Fig. 4.16 Changes in activation angle

Fig. 4.17 Horizontal force

finally α was increased by 30° and β was decreased by 60° . The springs will be referred to as springs 1 through 4.

The springs were mounted and tested as previously described, however due to the asymmetry of these springs the reactions at both ends were measured. Three tests were conducted for each end. The two ends of a spring will be referred to as the α end and the β end. Ideally, there should be a difference in moments at the α and β end which is equal to the product of a vertical force times the interbracket distance. The interbracket distances at the neutral position were found to be 10, 8, 10 and 15 mm.

Figures 4.17 to 4.22 show the horizontal force, vertical force, α moment, β moment, α moment to horizontal force ratio and β moment to horizontal force ratio. Figure 4.17 shows that the horizontal force was not effected to a large extent for the first, third and fourth springs; at a 7 mm deflection the force exerted by these three springs was .93, .88 and .82 times the force exerted by the 8 mm spring of the previous study. Increasing the α angle by 60° however caused the force to increase by 60 percent at a deflection of 2 mm. This spring began to yield at a deflection of 1.5-2 mm.

—The first spring (which possessed the least asymmetry) exerted the lowest vertical force and had the lowest difference in end moments (Figures 4.19 and 4.20). Decreasing the β angle caused the vertical force to increase considerably, although the third spring exerted a

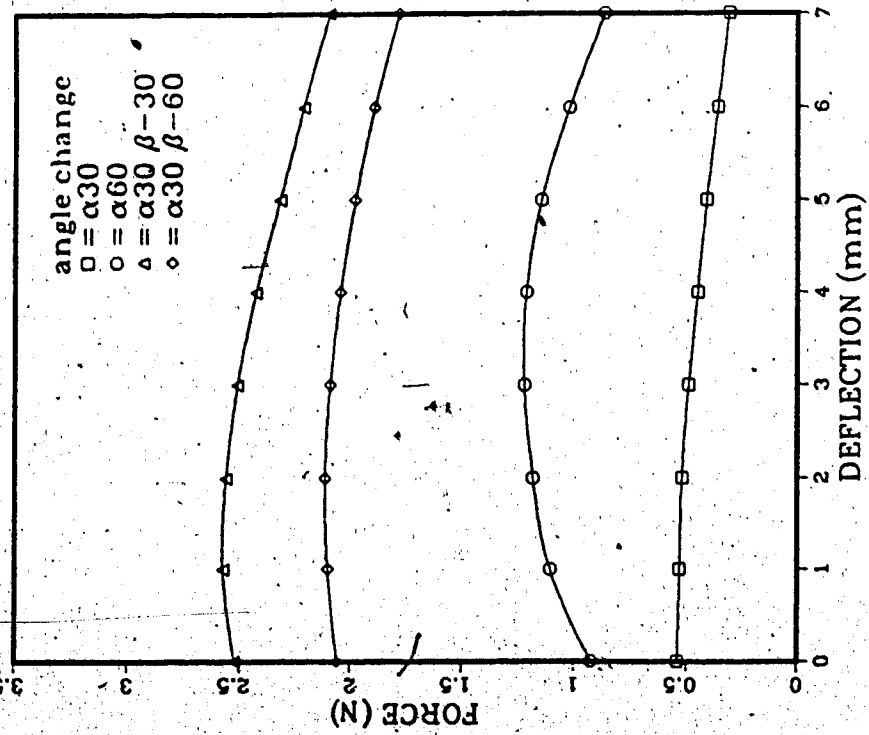


Fig. 4.18 Vertical force at α end

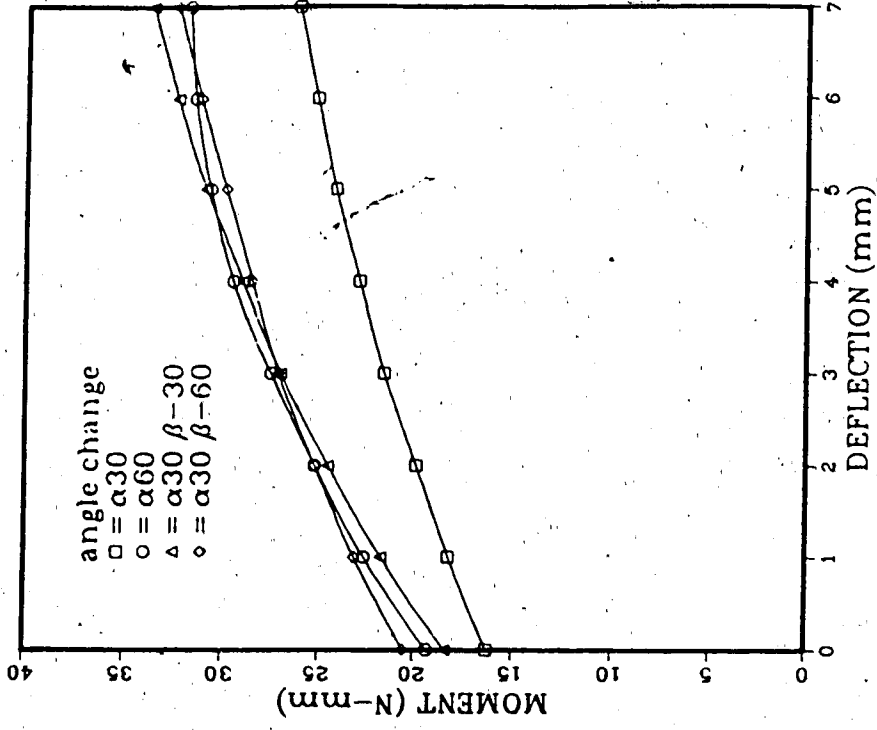


Fig. 4.19 Moment at α end

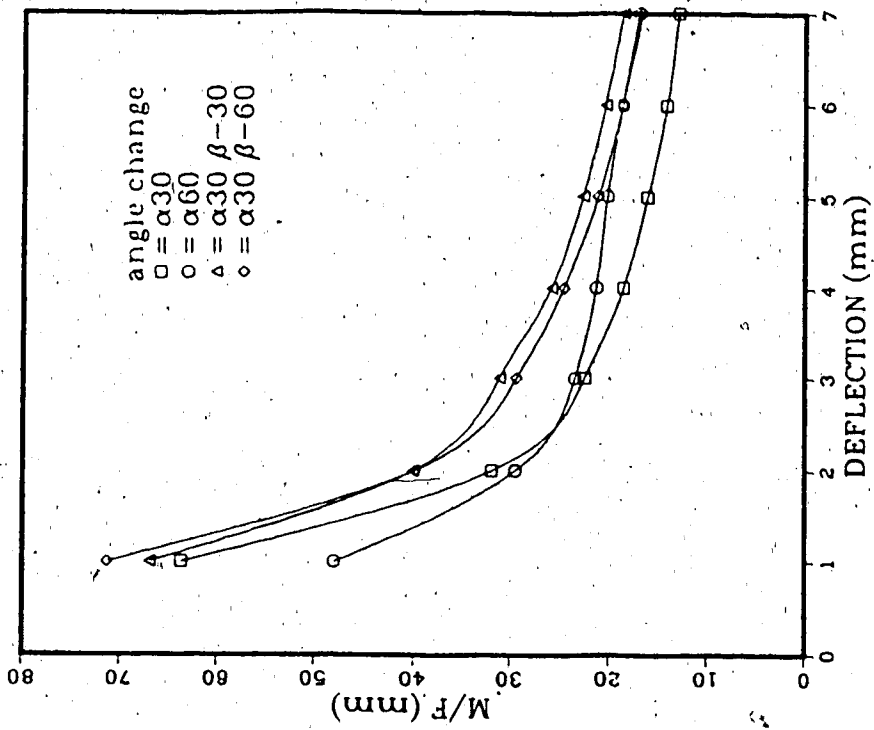


Fig. 4.21 Moment to force ratio at α end 19

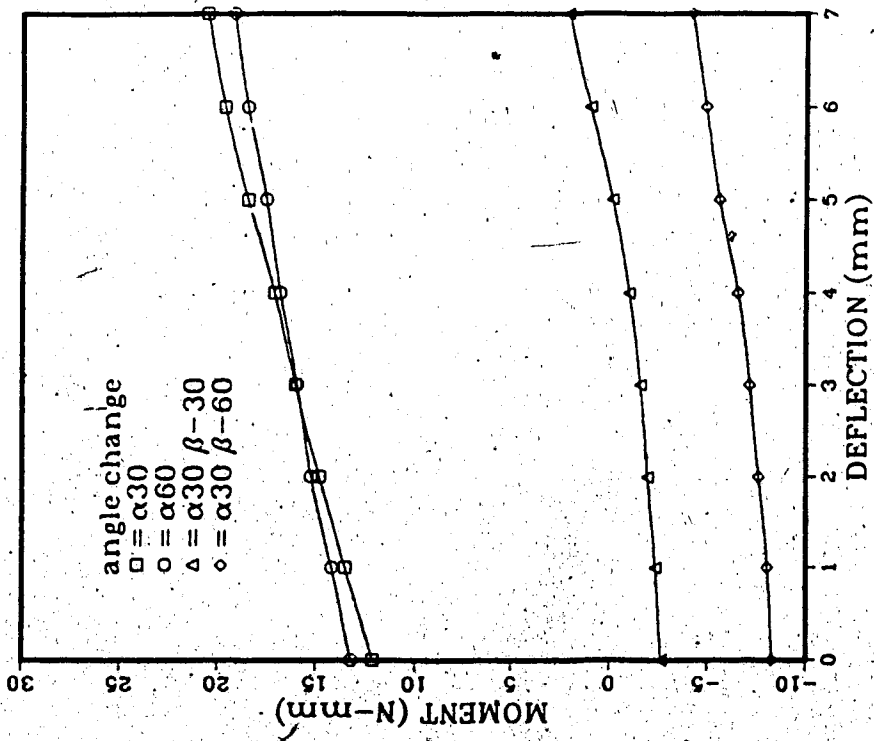


Fig. 4.20 Moment at β end

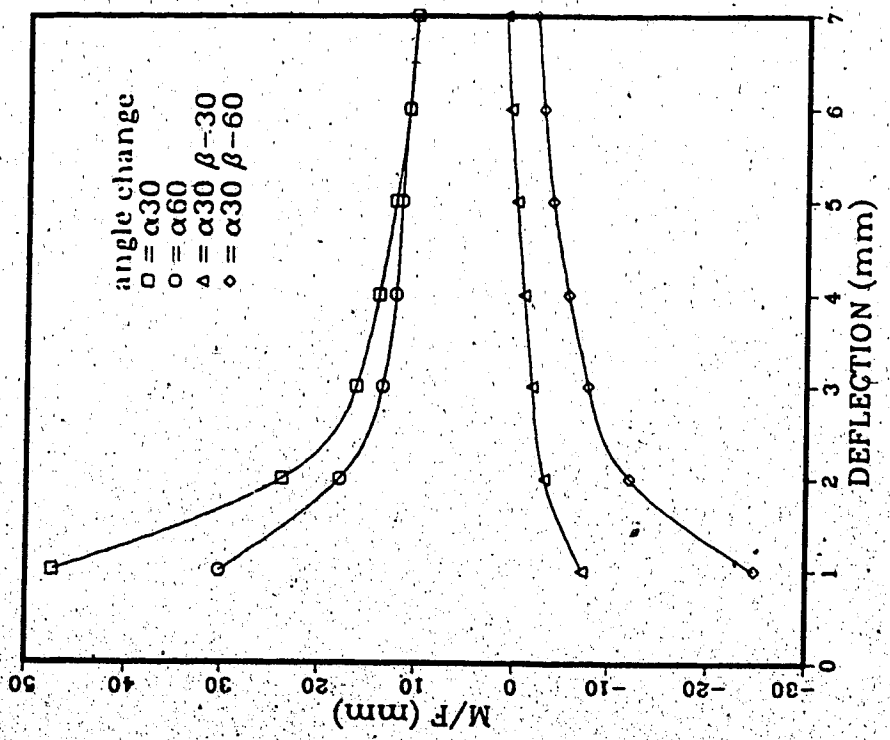


Fig. 4.22 Moment to force ratio at β end

larger vertical force than the fourth. As mentioned, it was also seen that the interbracket distances for spring 4 were 4 mm greater than for spring 3.

Referring to Figure 4.19, increasing the α angle from 30° to 60° and 90° (springs 1 and 2) increased the α moment by 20 percent and 50 percent. Comparing springs 1, 3 and 4 reveals that decreasing the β angle also caused an increase in α moment, however the effect is not directly proportional. From Figure 4.20 it is seen that decreasing the β angle from 30° to 0° and -30° (springs 3,4) lowers the β moment by 80 and 125 percent respectively. Comparing springs 1 and 2 and the symmetric 8 mm spring from the previous study reveals that increasing the α angle causes less than a 5 percent change in the β moment.

The α moment to horizontal force ratio is shown in Figure 4.21. It can be seen that the effect of increasing the α angle was to increase the α moment to force ratio (at higher activations). Also, decreasing the β angle raised the ratio but had little effect once the β angle became negative.

The β moment to horizontal force ratio is shown in Figure 4.22. The large difference in horizontal force delivered by spring 2 was responsible for lowering the moment to force ratio as the β moment was essentially unchanged between springs 1 and 2. The effect of decreasing the β angle past zero is seen in the negative β moment to force ratios for springs 2 and 3.

Finally, equilibrium was checked. As the vertical forces were most susceptible to misalignment, errors in vertical force are most likely the source of non-equilibrium. The difference in moments at the α and β ends was divided by the corresponding interbracket distance and subtracted from the vertical force. The maximum out-of-balance vertical forces for springs 1 through 4 were .136, .278, .098 and .153 N. Expressed as a percentage error of the corresponding vertical force the values are 25, 19, 11 and 7 percent. The standard deviations of the vertical force data remained below 7 percent. The value from deadweight tests was under 2 percent, indicating that most of the repeatability error encountered was due to misalignment and improper positioning of the springs in the instrument.

Case 3

Vertical forces and moment differences are also obtained when symmetric springs are not centered between brackets. The effect of spring offset was studied by testing the 8 mm spring clamped at a distance of 6 mm from the activation bends and subsequently offset by 2 and 4 mm towards the α side (Figure 4.23). The interbracket distances at the neutral position were found to be 22.5 mm for all three spring placements.

Figures 4.24 to 4.29 show the horizontal force,



Fig. 4.23 Variation in clamping points

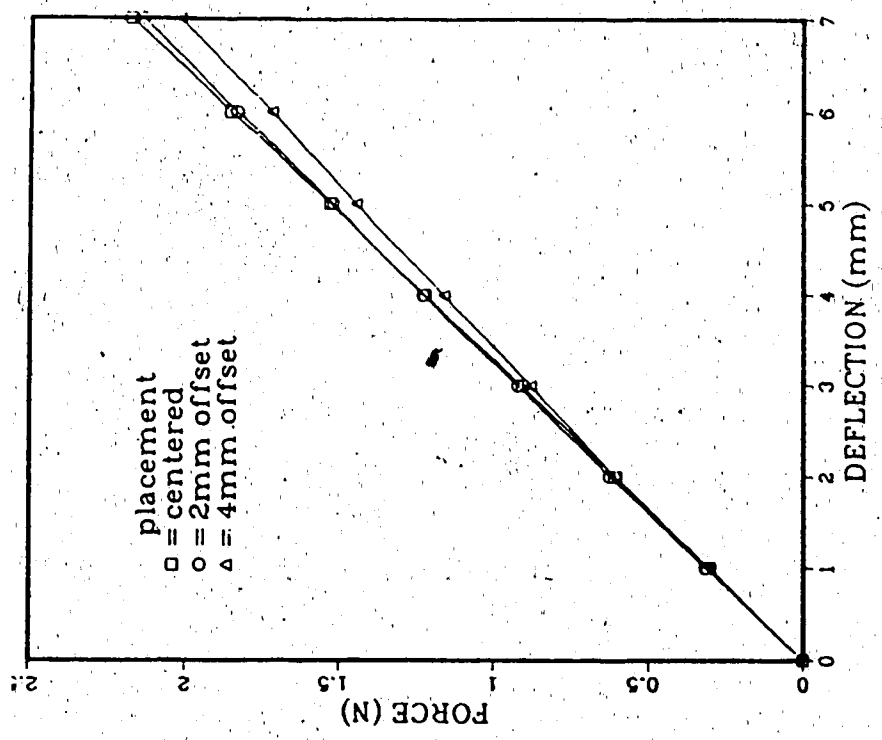


Fig. 4.24 Horizontal force

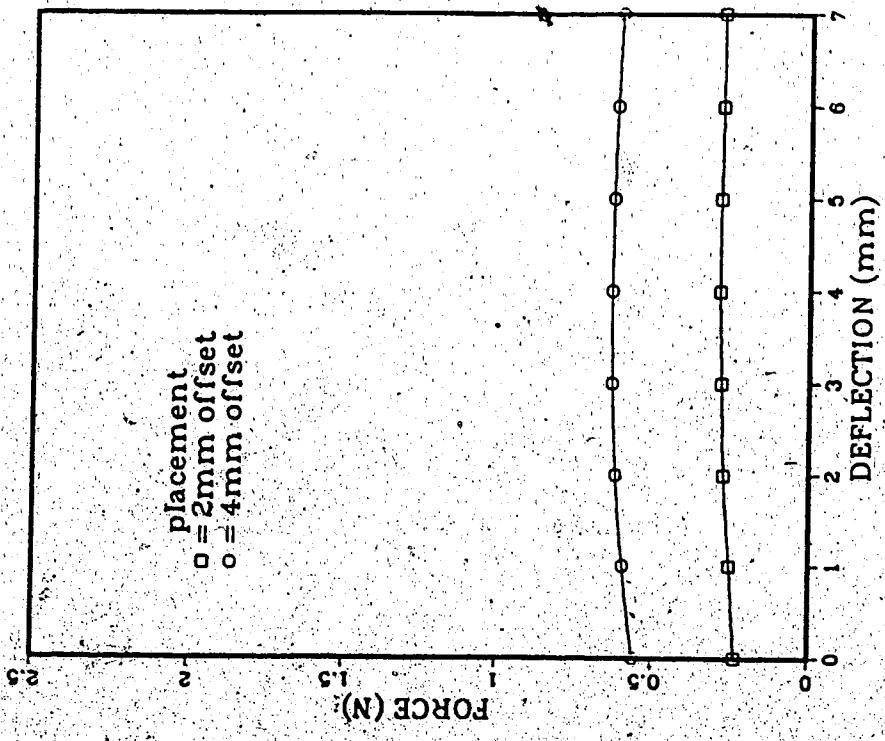


Fig. 4.25 Vertical force at α end

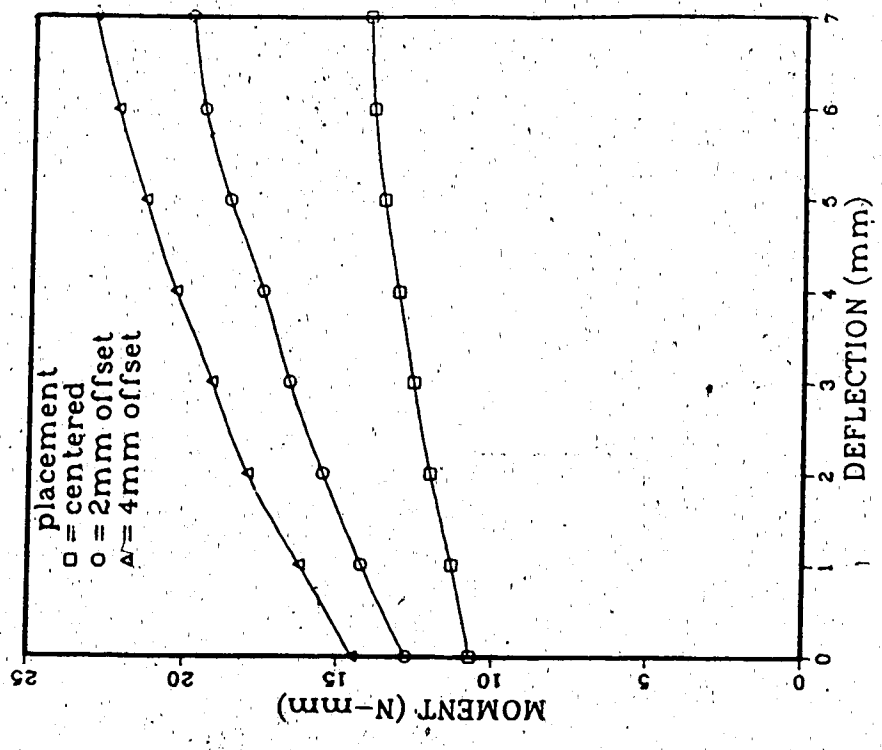


Fig. 4.26 Moment at α end

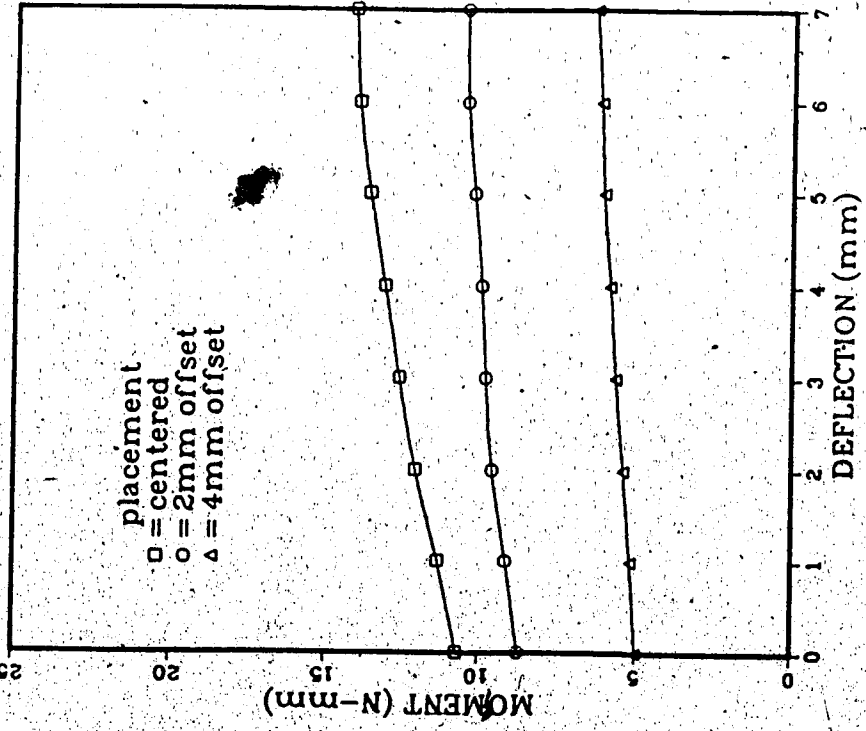


Fig. 4.27 Moment at β end

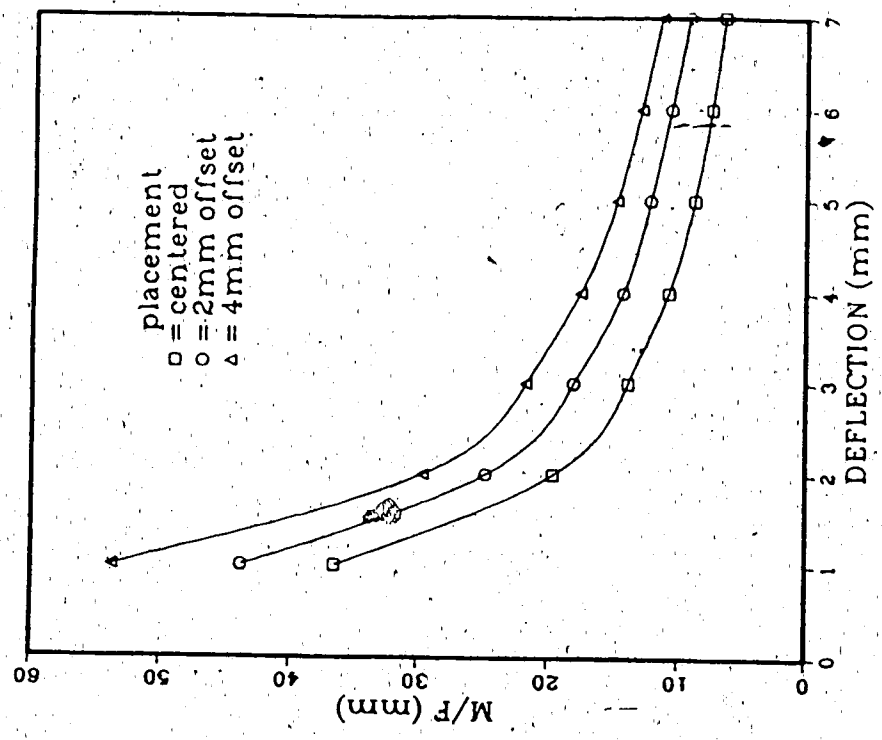


Fig. 4.28 Moment to force ratio at α end

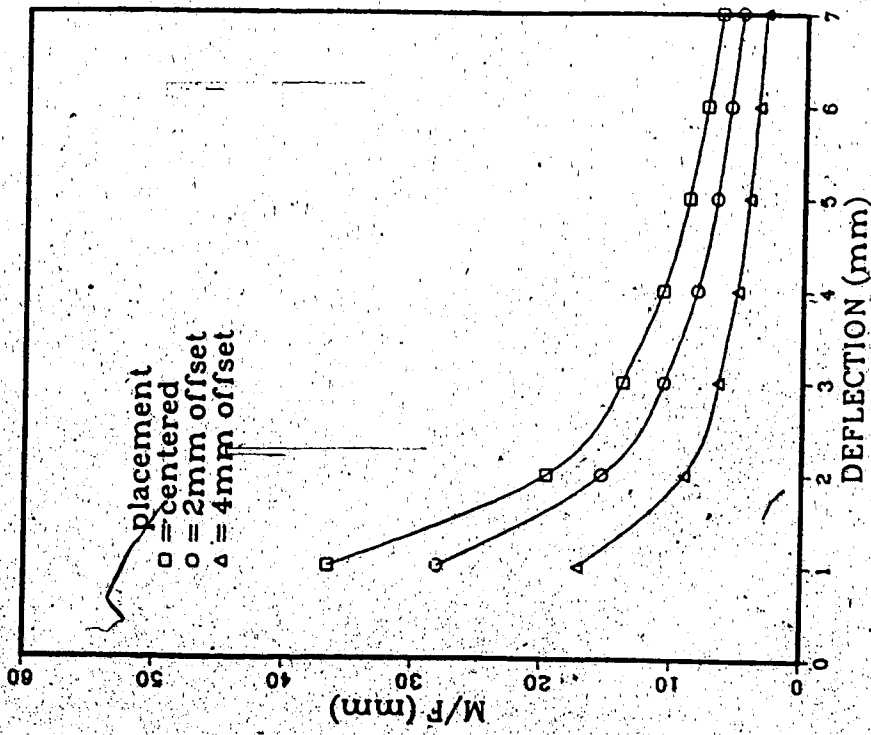


Fig. 4.29 Moment to force ratio at β end

vertical force, α moment, β moment, α moment to horizontal force ratio and β moment to horizontal force ratio. Figure 4.24 indicates that the horizontal force was unchanged by the 2 mm offset and is decreased by only 8 percent with the 4 mm offset. The vertical force resulting from a 2 mm offset was approximately 40 percent of the force delivered with a 4 mm offset throughout the activation (Figure 4.25).

The α and β moments are shown in Figures 4.26 and 4.27. The 2 mm and 4 mm offsets resulted in increases in α moment of 40 and 62 percent at a 7 mm deflection from the neutral position. The β moment experienced 25 and 55 percent decreases respectively. From Figures 4.28 and 4.29 the 2 and 4 mm offsets increased the α moment to force ratios by 20 and 45 percent. The β moment to force ratios were decreased by 25 and 32 percent.

Equilibrium was checked in the same manner as before. The largest out-of-balance vertical forces for the two placements were .04 and .06 N or 13 and 10 percent.

Case 4

The final parameter that was studied was the addition of helices. Two springs based on the 6 and 8 mm springs of the first study were constructed with single turns at each of the upper bends. The springs are shown in Figure 4.30.

Each spring was clamped 2 mm from the activation bends and tested as previously described. Four tests were

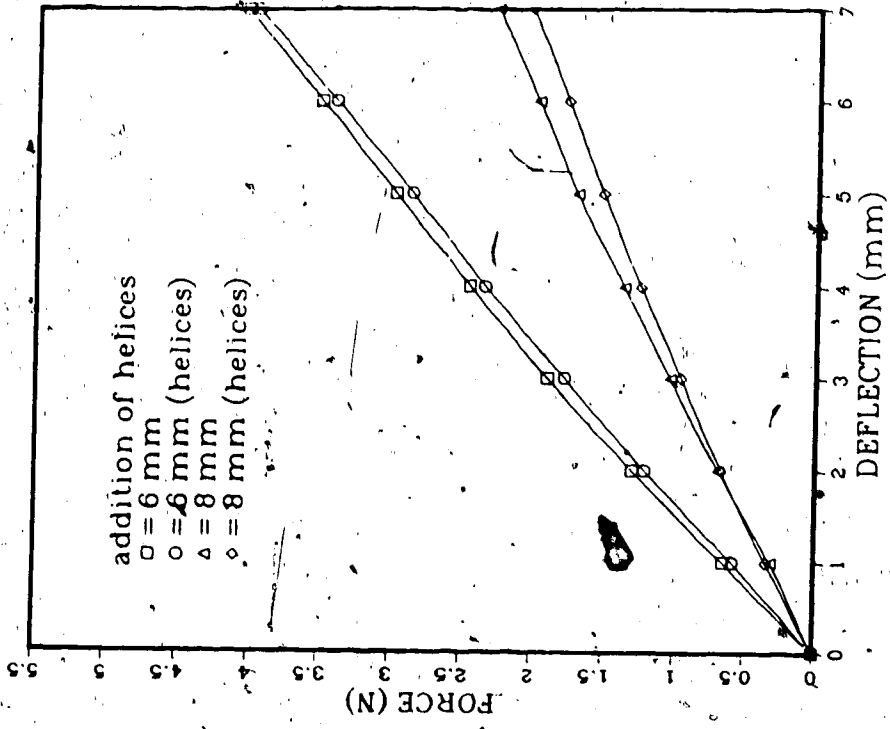


Fig. 4.31 Horizontal force-deflection relationship

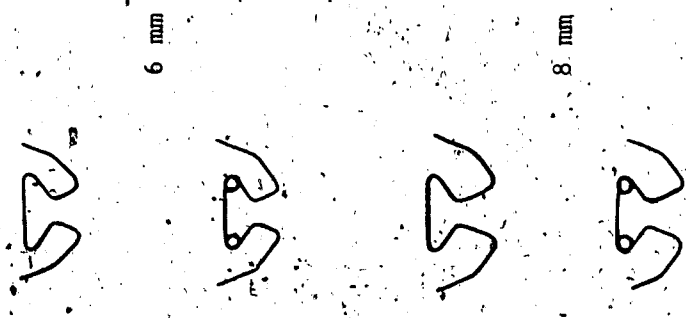


Fig. 4.30 Addition of helices

conducted for each spring. The interbracket distances at the neutral position were found to be 12 and 13 mm.

The horizontal force, moment and moment to force ratios are shown in Figures 4.31 to 4.33. The results show that the addition of helices at these locations lowers the force and moment delivered only slightly; at a 3 mm activation the forces were reduced by 4 and 9 percent and the moments by 4 and 7 percent for the 6 and 8 mm springs respectively.

Figure 4.33 shows that the moment to force ratio is effectively unchanged by the addition of these helices. It has generally been found that the addition of helices tends to further reduce the moment to force ratio at higher activations. It is expected that the addition of helices at the activation bends would result in a more noticeable effect.

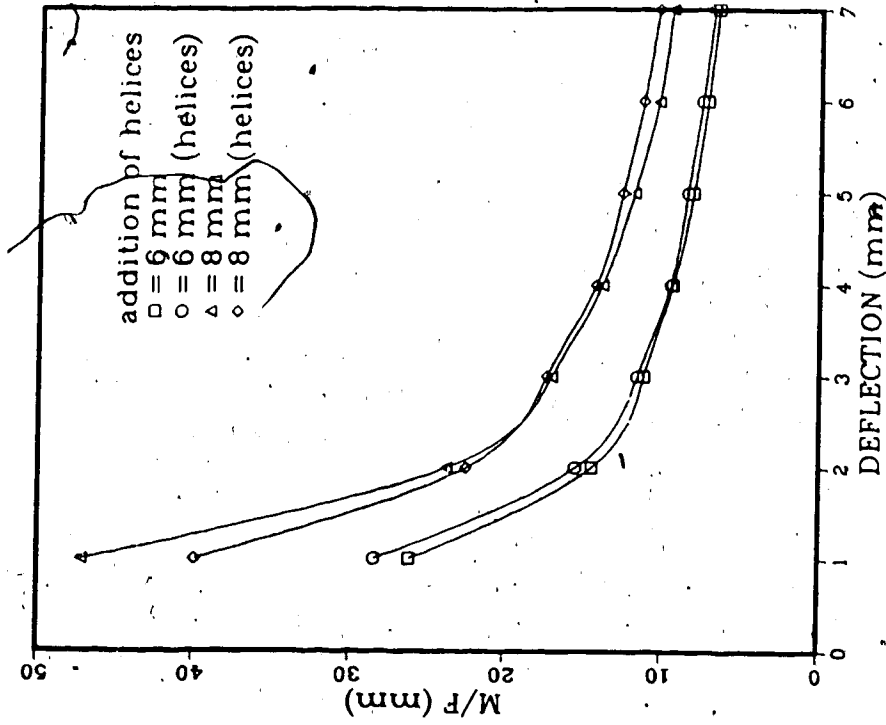


Fig. 4.33 Moment to force ratio

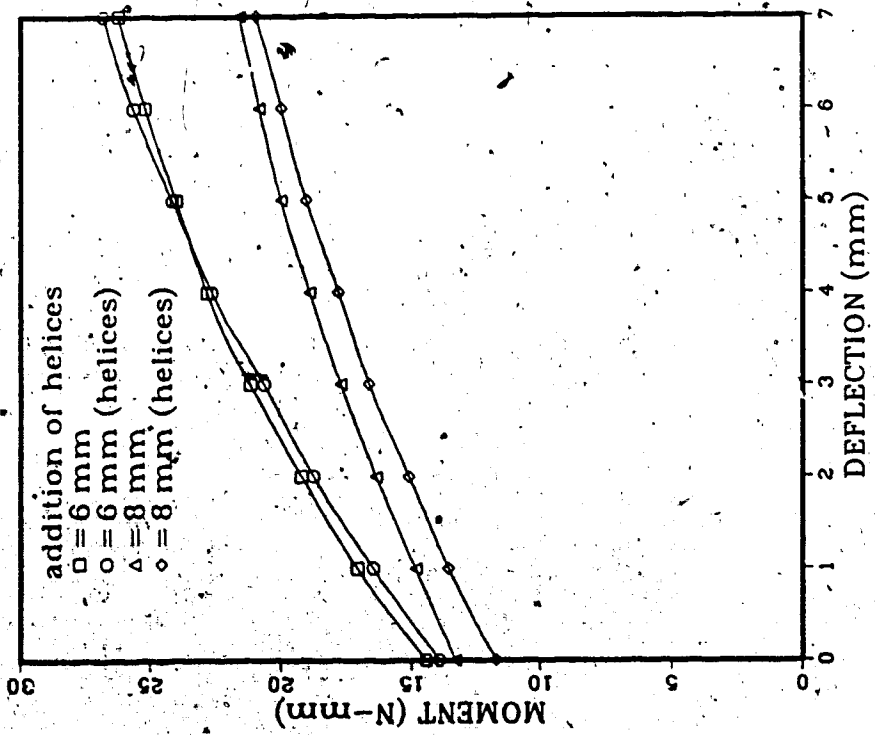


Fig. 4.32 Moment-deflection relationship

5. CONCLUSIONS

The focus of this study has been to apply and evaluate experimental and numerical techniques for determining the force systems generated by orthodontic appliances. A further objective was to gain insight into the effects of certain geometrical variations in the design of a T loop retraction spring. The following conclusions are drawn:

1. The instrument that was developed proved to be capable of measuring the force systems generated with sufficient accuracy and repeatability. The accuracy as determined from deadweight tests was 3.4 percent full scale. The standard deviations of data from spring tests remained below 7 percent, while the value from deadweight tests was under 2 percent.
2. Results from the finite element study have indicated that the method is an effective tool for modelling the appliances; however the cost of the analysis increases greatly as larger displacements and rotations are involved.
3. From the parametric study of a T loop design the following conclusions may be drawn. The reduction of height resulted in a larger increase in horizontal force generation than moment. Changing the activation angles as described did not affect the horizontal forces by a large amount, while creating a relatively large difference in vertical forces and moments. Increasing one of the angles and decreasing the other resulted in the greatest

asymmetry. Increasing the α angle by 60° caused a similar increase in the α moment as increasing the α angle by 30° and decreasing the β angle by 30° (and 60°). Finally, increasing the α angle had very little effect on the β moment, and decreasing the β angle reduced the β moment proportionally. Mounting the spring further towards the α bracket resulted in little change in the horizontal force and proportional increases in the vertical force and moment at the α end. The addition of helices at the top of the spring served to lower the forces and moments by only minor amounts.

Most of the repeatability error encountered was due to misalignment and improper positioning of the spring in the instrument. An improvement in alignment would increase the accuracy and ease in gathering data. This could be achieved by designing a base for the instrument upon which the displacement transducers could be permanently mounted. Once the initial alignment was completed the instrument could be easily zeroed without having to rely on optical methods such as the use of a cathetometer. The problem of mounting the spring at exactly the right position and orientation would however, still remain.

As mentioned, the computing costs increase greatly as larger displacements and rotations are involved. The first study that was conducted had an execution time of seven minutes while the second case took two and a quarter hours to achieve a similar level of convergence. A more

economical alternative for this case may lie in the use of fewer elements or simpler elements such as the straight Hermitian beam element, although this would result in a compromise of accuracy.

Future areas of study include the testing and modelling of the appliance-tooth connection conditions at the bracket. An experimental study of the entire appliance-tooth-support structure system is difficult due to problems encountered in the preparation of artificial materials to match the mechanical properties of biological tissues. An experimental study involving only the appliance and brackets could be conducted however, to determine the actual force systems delivered to the tooth.

REFERENCES

1. Solonche, D.J., Burstone, C.J. and Vanderby, R., "A Device for Determining Force-Moment Characteristics of Orthodontic Appliances", IEEE Transactions on Engineering in Medicine and Biology, BME 24(6), 1977, pp. 538-539.
2. Koenig, H. A., Burstone, C. J., "Analysis of Generalized Curved Beams for Orthodontic Applications", Journal of Biomechanics, vol. 7, 1974, pp. 429-435.
3. Peyton, S.A. and Moore, G.R., "Measuring the Forces of Displacement in Orthodontic Spring Appliances", International Journal of Orthodontics, vol. 19, 1933, pp. 683-686.
4. Paulich, S., "Measuring of Orthodontic Forces", American Journal of Orthodontics and Oral Surgery, vol. 25, 1939, pp. 817-849.
5. Johns, E.E., "A Study of the Forces Inherent in Orthodontic Appliances and Selection of Forces for Tooth Movement", Journal of Canadian Dental Association, vol. 19, 1953, pp. 423-436.
6. Teasly, G.H., Penley, W. and Morrison E., "The Design and Fabrication of an Electronic Instrument to Analyze Orthodontic Forces", American Journal of Orthodontics, vol. 49, 1953, p. 868 (abstract).
7. Paquien, J., "The Measurement of Forces and Moments Delivered by Dental Appliances", M. Sc. Thesis, The University of Manitoba, 1978.
8. Koenig, H.A., Vanderby, R., Solonche, D.J. and Burstone C.J., "Force Systems from Orthodontic Appliances: An Analytical and Experimental Comparison", Journal of Biomechanical Engineering, vol. 102, 1980, pp. 294-300.
9. Sachdeva, R.C., "A Study of Force Systems Produced by TMA 'T' Loop Retraction Springs", M. Sc. Thesis, University of Connecticut, 1983.
10. Solonche, D.J., Burstone, C. J. and Ratches, J., "A Computer Controlled Device for Determining the Mechanical Behaviour of Orthodontic Appliances", abstract, 30th Annual Conference on Engineering in Medicine and Biology, Los Angeles, Calif., Nov. 1977.

11. Sullivan, D.J., "An Investigation into the Three-Dimensional Force and Moment Characteristics of Selected Low-Modulus Initial Alignment Archwires", M. Sc. Thesis, University of Manitoba, 1982.
12. Lack, M.L., "An Investigation into the Three-Dimensional Force and Moment Characteristics of Selected Cuspid Retraction Mechanisms", M. Sc. Thesis, University of Manitoba, 1980.
13. Waters, N.E., "The Mechanics of Plain and Looped Arches", British Journal of Orthodontics, vol. 3, no. 3, 1975, pp. 161-167.
14. Yang, T.Y., "Matrix Displacement Solution Elastica Problems of Beams and Frames", International Journal of Solids and Structures, vol. 9, 1973, pp. 829-842.
15. Yang, T.Y. and Baldwin, J.J., "Analysis of Space Closing Springs in Orthodontics", Journal of Biomechanics, vol. 7, 1974, pp. 21-28.
16. von Trostel, R., "Contribution to the Study of Spatial Curved Beams by the Theory of the First Order", Ing. Archiv., vol. 25, 1957.
17. Suhubi, E.S., "On the Foundations of the Theory of Rods", International Journal of Engineering Science, vol. 6, 1968, pp. 169-191.
18. Massoud, M.F., "A Generalized Formulation of the Vectorial Equations of Motion for Non-Prismatic Thin Space Beams", Journal of Applied Mechanics, ASME, Paper No. 71-APM-P, 1971.
19. Greif, R., Coltman, M., Gailus, M. and Shapiro, E., "Force Generation from Orthodontic Appliances", Journal of Biomechanical Engineering, vol. 104, 1982, pp. 280-289.
20. Bathe, K.J., "Finite Element Procedures in Engineering Analysis", Prentice-Hall, 1982.
21. "ADINA Theory and Modelling Guide", ADINA Engineering Report AE 84-4, 1984.
22. Yoshikawa, D.K., Burstone, C.J., Goldberg, A.J., and Morton, J., "Flexure Modulus of Orthodontic Stainless Steel Wires", Journal of Dental Research, vol. 60, 1981, pp. 139-145.

23. Goldberg, A.J., Morton, J. and Burstone, C.J., "The Flexure Modulus of Elasticity of Orthodontic Wires", Journal of Dental Research, vol. 62(7), 1983, pp. 856-858.

APPENDIX - TEST RESULTS

DEFL. (mm)	AVERAGE VALUES		STANDARD DEVIATIONS	
	FH (N)	M (N-mm)	FH (N)	M (N-mm)
0	0	0	0	0
0.25	0.228	0.87	.006	.03
0.50	0.465	1.78	.008	.04
0.75	0.661	2.51	.011	.07
1.0	0.840	3.20	.015	.08
1.25	1.024	3.87	.024	.11
1.50	1.205	4.55	.027	.12
1.75	1.368	5.20	.031	.12
2.0	1.531	5.82	.029	.14

DEFL. (mm)	FH (N)	M (N-mm)	FH (N)	M (N-mm)
0	0	12.57	0	.41
1	0.190	14.21	.010	.72
2	0.375	15.74	.015	.83
3	0.574	17.19	.023	.76
4	0.762	18.46	.026	.82
5	0.925	19.69	.031	.75
6	1.104	20.83	.040	.78
7	1.272	21.88	.041	.62

Table A.1 Results from comparative studies

DEFL. (mm)	AVERAGE		VALUES		STANDARD		DEVIATIONS	
	FH (N)	M (N-mm)	FH (N)	M (N-mm)	FH (N)	M (N-mm)	FH (N)	M (N-mm)
height (mm)								
0	0	15.42	0	14.44	0	.47	0	.43
1	1.13	18.78	.652	17.08	.017	.42	.013	.41
2	2.26	21.25	1.327	19.19	.038	.48	.022	.45
3	3.39	23.26	1.892	21.17	.066	.54	.031	.49
4	4.52	24.69	2.451	22.83	.087	.59	.059	.53
5	5.65	25.65	2.984	24.08	.090	.53	.067	.57
6	6.78	26.43	3.514	25.39	.115	.58	.072	.53
7	7.91	27.15	4.042	26.21	.137	.64	.096	.52
height (mm)								
0	0	13.63	0	13.28	0	.41	0	.39
1	.458	15.42	.315	14.85	.015	.40	.014	.35
2	.931	17.37	.687	16.36	.024	.38	.019	.42
3	1.323	19.08	1.043	17.72	.027	.49	.023	.46
4	1.748	20.64	1.369	18.90	.035	.42	.031	.41
5	2.143	21.86	1.690	20.04	.048	.44	.042	.42
6	2.549	22.99	1.982	20.88	.074	.45	.054	.48
7	2.917	24.02	2.285	21.64	.097	.42	.061	.46
DEFL. (mm)	M/FH (mm)	M/FH (mm)	M/FH (mm)	M/FH (mm)	M/FH (mm)	M/FH (mm)	M/FH (mm)	M/FH (mm)
height (mm)								
0								
1	16.65	26.20	33.67	47.14				
2	10.20	14.46	18.66	23.81				
3	8.09	11.19	14.45	16.99				
4	6.77	9.31	11.81	13.80				
5	6.06	8.07	10.20	11.86				
6	5.63	7.17	9.02	10.53				
7	5.22	6.49	8.23	9.47				

Table A.2 Results from spring height study

AVERAGE		VALUES		STANDARD		DEVIATIONS		
DEFL. (mm)	FH (N)	FV (N)	M _α (N-mm)	M _β (N-mm)	FH (N)	FV (N)	M _α (N-mm)	M _β (N-mm)
angle change (deg.)								
α30								
0	0	.545	16.25	12.15	0	.046	.27	.36
1	.287	.532	18.24	13.57	.015	.050	.29	.39
2	.623	.527	19.88	14.78	.017	.041	.35	.41
3	.925	.486	21.63	15.93	.026	.045	.38	.38
4	1.236	.451	22.90	17.18	.031	.052	.29	.43
5	1.501	.409	24.18	18.36	.034	.061	.36	.32
6	1.783	.368	25.23	19.42	.041	.056	.34	.36
7	2.024	.316	26.27	20.53	.042	.044	.38	.35
α60								
0	0	.916	19.28	13.25	0	.052	.46	.42
1	.472	1.127	22.64	14.27	.016	.049	.43	.41
2	.854	1.181	25.18	15.25	.018	.057	.48	.44
3	1.179	1.224	27.53	15.88	.021	.053	.39	.42
4	1.382	1.217	29.48	16.79	.020	.078	.45	.40
5	1.512	1.145	30.60	17.54	.018	.054	.48	.38
6	1.684	1.020	31.47	18.41	.022	.062	.41	.36
7	1.874	.871	31.82	19.14	.023	.059	.38	.46
α30β-30								
0	0	2.523	18.44	-2.64	0	.057	.54	.32
1	.325	2.575	21.73	-2.36	.023	.049	.42	.36
2	.613	2.561	24.56	-1.97	.020	.055	.40	.43
3	.869	2.510	27.08	-1.61	.026	.058	.61	.51
4	1.125	2.427	29.07	-1.03	.025	.067	.59	.43
5	1.368	2.320	30.95	-.16	.028	.054	.53	.45
6	1.584	2.215	32.42	.695	.029	.062	.56	.47
7	1.813	2.102	33.79	2.02	.031	.068	.54	.42
α30β-60								
0	0	2.062	20.51	-8.27	0	.081	.34	.43
1	.325	2.104	23.17	-8.04	.021	.069	.41	.45
2	.633	2.116	25.23	-7.61	.031	.065	.30	.38
3	.921	2.094	27.10	-7.15	.032	.072	.35	.35
4	1.164	2.045	28.52	-6.58	.029	.056	.37	.31
5	1.416	1.978	29.95	-5.63	.032	.063	.32	.37
6	1.673	1.892	31.23	-4.93	.031	.073	.47	.32
7	1.938	1.783	32.41	-4.23	.038	.075	.38	.40
DEFL. (mm)	M _α /FH (mm)	M _β /FH (mm)	M _α /FH (mm)	M _β /FH (mm)	M _α /FH (mm)	M _β /FH (mm)	M _α /FH (mm)	M _β /FH (mm)
angle change (deg.)								
	α30		α60		α30β-30		α30β-60	
0								
1	63.55	47.28	47.97	30.23	66.86	-7.26	71.29	-24.74
2	31.91	23.72	29.48	17.86	40.07	-3.21	39.86	-12.02
3	23.38	17.22	23.35	13.47	31.16	-1.85	29.40	-7.76
4	18.53	13.90	21.33	12.15	25.84	-0.92	24.50	-5.65
5	16.11	12.23	20.24	11.60	22.62	-0.12	21.15	-3.98
6	14.15	10.89	18.69	10.93	20.47	0.60	18.67	-2.95
7	12.98	10.14	16.98	10.21	18.64	1.11	16.72	-2.18

Table A.3 Results from activation angle study

DEFL. (mm)	FH (N)	AVERAGE		VALUES		STANDARD		DEVIATIONS	
		FV (N)	M _a (N-mm)	M _β (N-mm)	FH (N)	FV (N)	M _a (N-mm)	M _β (N-mm)	
placement:									
centered									
0	0		10.70		0			.12	
1	.310		11.32		.012			.17	
2	.614		12.05		.014			.18	
3	.908		12.60		.018			.21	
4	1.217		13.10		.021			.23	
5	1.532		13.58		.026			.19	
6	1.853		13.96		.030			.09	
7	2.176		14.11		.032			.07	
2 mm offset									
0	0	.274	8.72	12.75	0	.012	.11	.14	
1	.325	.298	9.13	14.24	.008	.014	.15	.16	
2	.624	.316	9.59	15.50	.010	.017	.18	.17	
3	.923	.325	9.81	16.65	.013	.018	.20	.19	
4	1.228	.331	9.98	17.54	.019	.021	.21	.21	
5	1.524	.331	10.22	18.59	.023	.023	.23	.19	
6	1.827	.329	10.49	19.45	.027	.019	.20	.21	
7	2.143	.327	10.54	19.90	.030	.018	.17	.19	
4 mm offset									
0	0	.557	4.99	14.93	0	.015	.15	.16	
1	.302	.596	5.19	16.22	.012	.019	.16	.20	
2	.605	.621	5.46	17.96	.015	.024	.19	.19	
3	.881	.633	5.70	19.15	.020	.027	.18	.24	
4	1.160	.636	5.90	20.36	.022	.032	.21	.23	
5	1.443	.632	6.12	21.37	.026	.030	.24	.26	
6	1.723	.623	6.23	22.29	.031	.031	.23	.24	
7	2.024	.610	6.41	23.07	.032	.028	.22	.21	
DEFL. M/FH M _a /FH M _β /FH M _a /FH M _β /FH									
placement:									
centered 2 mm offset 4 mm offset									
0									
1		36.52	28.09	43.82		17.19	53.71		
2		19.63	15.37	24.84		9.02	29.69		
3		13.88	10.63	18.04		6.47	21.74		
4		10.76	8.13	14.28		5.09	17.55		
5		8.86	6.71	12.20		4.24	14.81		
6		7.53	5.74	10.65		3.62	12.94		
7		6.48	4.92	9.29		3.18	11.40		

Table A.4 Results from placement study

DEFL. (mm)	AVERAGE		VALUES		STANDARD		DEVIATIONS	
	FH (N)	M (N-mm)	FH (N)	M (N-mm)	FH (N)	M (N-mm)	FH (N)	M (N-mm)
height (mm)	6		6 (helices)		6		6 (helices)	
0	0	14.44	0	13.91	0	.43	0	.63
1	.652	17.08	.576	16.47	.013	.41	.022	.75
2	1.327	19.19	1.210	18.73	.022	.45	.031	.82
3	1.892	21.17	1.783	20.65	.031	.49	.044	.87
4	2.451	22.83	2.339	22.63	.059	.53	.054	.83
5	2.984	24.08	2.857	24.14	.067	.57	.079	.85
6	3.514	25.19	3.412	25.67	.072	.53	.089	.80
7	4.042	26.21	3.958	26.80	.096	.52	.083	.84
height (mm)	8		8 (helices)		8		8 (helices)	
0	0	13.28	0	11.69	0	.39	0	.52
1	.315	14.85	.344	13.55	.014	.35	.019	.67
2	.687	16.36	.671	15.10	.019	.42	.022	.61
3	1.043	17.72	.958	16.63	.023	.46	.028	.74
4	1.369	18.90	1.252	17.78	.031	.41	.037	.68
5	1.690	20.04	1.518	19.04	.042	.42	.055	.64
6	1.984	20.86	1.774	20.02	.054	.48	.062	.71
7	2.285	21.64	2.032	21.14	.061	.46	.074	.62
DEFL. (mm)	M/FH (mm)	M/FH (mm)	M/FH (mm)	M/FH (mm)	M/FH (mm)	M/FH (mm)	M/FH (mm)	M/FH (mm)
height (mm)	6		6 (helices)		8		8 (helices)	
0								
1	26.20	28.60	47.14	89.39				
2	14.46	15.48	23.81	22.50				
3	11.19	11.58	16.99	17.36				
4	9.31	9.67	13.80	14.20				
5	8.07	8.45	11.86	12.54				
6	7.17	7.52	10.51	11.29				
7	6.49	6.77	9.47	10.40				

Table A.5 Results from helices study